DEPARTMENT OF
MINERALS AND ENERGY

# BUREAU OF MINERAL RESOURCES, GEOLOGY AND GEOPHYSICS



Record 1974/150



## SIDE-LOOKING AIRBORNE RADAR FOR GEOLOGY:

## General principles, interpretation methods and evaluation at Mt Isa

by

C. MAFFI

Bur. Min. Resour. Aust. Rec. 1974/150

CORRECTIONS

| Page | Line | The words | Should read |
|---|---|---|---|
| 14 | 10 | p. 149V. | p. 149). |
| 18 | 31 | (page 31) | (page 30) |
| 21 | 24 | swamps are | swamps (S) are |
| 27 | 36 | and an | and on |
| 30 | 20 | Mt Isa was | Mt Isa area was |
| 33 | 19 | driection | direction |
| 34 | 23 | coul | could |
| 34 | 35 | dimensions | directions |
| 35 | 5 and 7 | Ultrapham | Ultraphan |
| 36 | last | trace | traced |
| 39 | 23 | me | ~~C~~me |
| 39 | 24 | mi | ~~C~~mi |
| 41 | last-1 | rainage | drainage |
| 43 | 3 | contrast | constant |
| 43 | 4 | ther | the |
| 43 | last | woul | would |
| 44 | 7 | defecting | detecting |
| Fig. 25 (between pages 33 and 34)-last line of legend | | (Figs 26, 27, 28) | (Plate 1) |

Record 1974/150

# SIDE-LOOKING AIRBORNE RADAR FOR GEOLOGY:

## General principles, interpretation methods and evaluation at Mt Isa

by

C. MAFFI

CONTENTS

## SUMMARY

Side Looking Airborne Radar (SLAR) systems are described in simple terms. Interpretation methods are given using examples of imagery from Papua New Guinea and from the Mt Isa area. The detailed interpretation of experimental SLAR imagery from the Mt Isa area has:

a) confirmed the well known SLAR properties such as all-weather capability, uniformity of illumination direction, emphasis on effect of relief, synoptic view of terrain, and suitability for reconnaissance geological mapping;

b) shown that generally sandstones, quartzites, intrusive rocks, and volcanic rocks can easily be interpreted; shales, siltstones, and schists are difficult to separate;

c) shown that SLAR imagery is particularly suitable for structural interpretation. Some previously unmapped faults and lineaments are visible in the imagery; copper mineralization may be associated with one of them;

The cost effectiveness of SLAR in Australian semi-arid environments depends on the importance that some of its properties - the combination of relief enhancement with synoptic view of the terrain, and the capability of detecting linear features that would be difficult or impossible to detect on aerial photographs or on satellite images - may have for the solution of the particular problem being considered.

A comprehensive list of publications on SLAR theory and on its applications to geology and related sciences is given.

# 1. INTRODUCTION

Remote sensing has become an important tool for the earth scientist. During the last 30 years, a large range of equipment has become available, which operates in the invisible as well as in the visible bands of the electromagnetic spectrum. In addition to aerial cameras this equipment includes infrared scanners, multi-spectral scanners, laser profilers, and side-looking radar. These sensors can be broadly grouped into two types: active and passive. The active sensors provide their own source of energy; the passive sensors use energy emitted from natural sources.

Side Looking Airborne Radar (SLAR) is an active system, operating in the millimetre and centimetre bands of the electromagnetic spectrum. Being an active system, it is not affected by diurnal and seasonal changes in the radiation emitted or reflected from the Earth's surface. As it operates at microwave frequencies, it is little susceptible to atmospheric conditions.

Because of these properties, SLAR has proved extremely useful for mapping tropical regions. For example, in 1967 the Darien Province of Panama was imaged from four different look directions in six days of operation; in the 15 years before the radar mission, continuous effort had resulted in spotty airphoto coverage of only 30 percent of the province, because of cloud cover (Rouse et al., 1969).

For the same reasons, SLAR is useful for mapping polar regions, where not only weather but also sun elevation may constrain aerial photography (Anderson, 1966; Leighty, 1966).

To assess the usefulness of SLAR in an arid region, BMR and the Division of National Mapping (DNM) launched in 1972 a joint project. An area of about 10 000 $km^2$ in the Mt Isa/Cloncurry region was flown in June of that year by Canadian Aero Services; the aircraft was a twin-jet Caravelle, equipped with a Goodyear radar system model GEMS 1000. BMR carried out the geological evaluation of the imagery.

The main purpose of this report is to describe how the investigation was carried out and its results. A description of the basic principles of SLAR and a discussion of SLAR interpretation methods is also given to gather information scattered in several books and publications.

# 2. GENERAL INFORMATION ON SIDE-LOOKING RADAR

The name RADAR comes from RAdio Detection And Ranging. Radar detection of an object is achieved by transmitting a beam of radio-frequency energy and detecting the energy reflected by the object. Radar-ranging is

accomplished by measuring the time required for the radio-frequency energy to make the round trip.

Side Looking Airborne Radar (SLAR) is a particular application of the general radar principle. A SLAR system is essentially composed of a transmitter, an aerial, and a receiver. The transmitter produces electromagnetic (em) radiation which is directed by the aerial sideways from the aircraft towards the ground (Fig. 1). The echoes from objects on the ground return to the

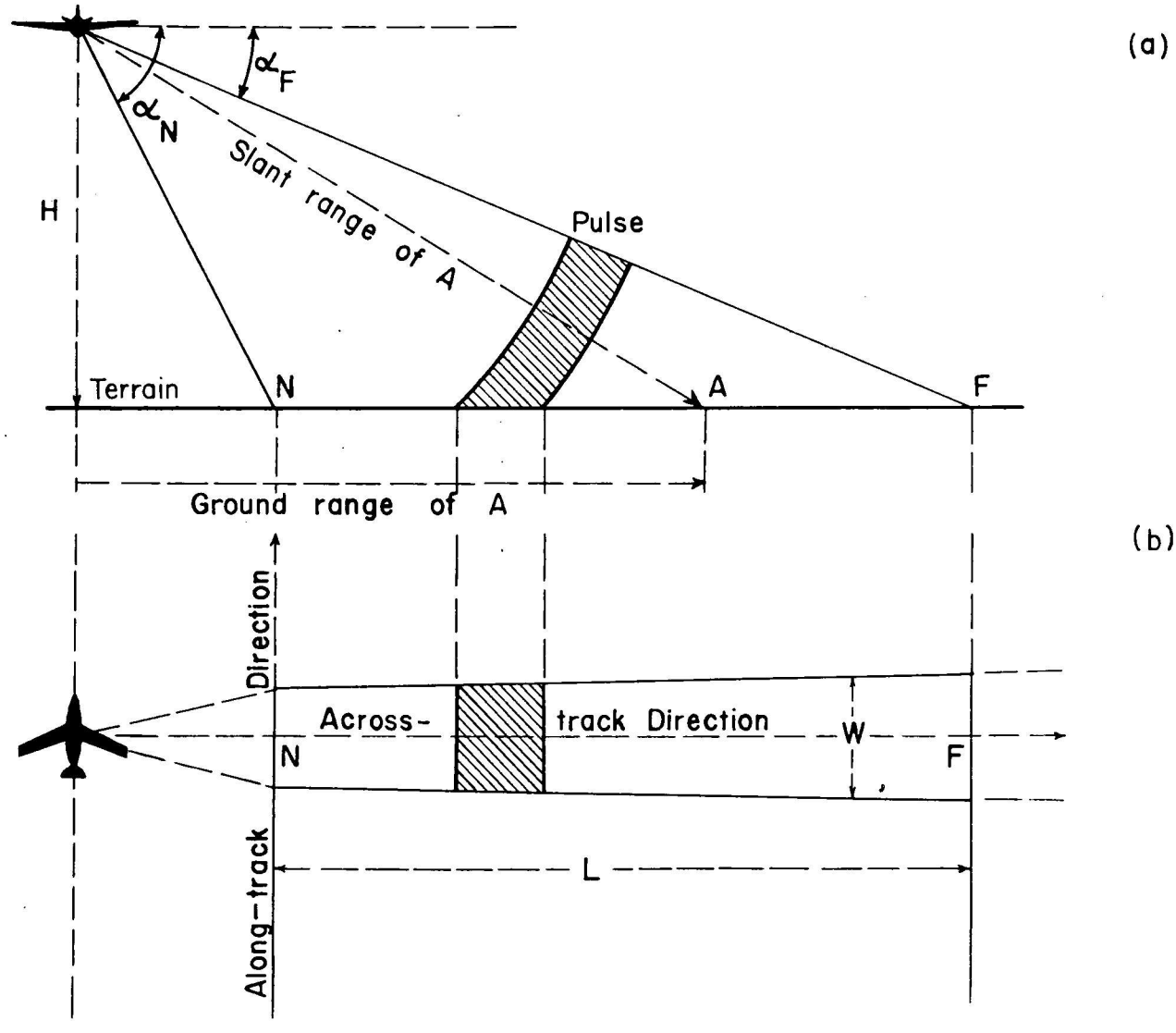


Fig 1 - Basic geometry

aerial and are conveyed to the receiver. The time elapsed between transmission and reception, and the intensity of the received signals are

processed to obtain a map-like display of the objects.

## BASIC GEOMETRY

The emission of electromagnetic radiation is not continuous, but is done in short pulses. The length of a pulse is about 1 microsecond, and the pulse repetition frequency (prf) is about 1000 per second. Each pulse travels away from the aircraft at a velocity very close to the velocity of light. The shaded area in Figure 1a indicates the position of such a pulse at a given instant. At this instant the ground element from which the energy is returned to the radar is the shaded area in Figure 1b. During the interval between two consecutive transmission pulses, the small reflecting zone travels from N (near range) to F (far range), thus covering a swath of width W and length L. Because of this scanning action, echoes from objects at different ranges from the aircraft reach the aerial at different times and can be recorded separately.

The scanning action is a result of the obliquity of the beam. If the beam was vertical, the echoes from all the objects equidistant from the nadir point of the aircraft would reach the aerial at the same time and the system would not be able to separate them.

As the aircraft moves forward, successive pulses are released and a continuous strip of terrain of width L is covered. Obviously L depends on the flight altitude above the ground, H, and the depression angles at near and far ranges, $\alpha_N$ and $\alpha_F$. For example the Mt Isa/Cloncurry imagery was flown with H = 9000 m, $\alpha_N = 45°$ and $\alpha_F = 15°$; thus each strip covers an area 24 km wide.

When a large area has to be covered, it may be necessary to fly parallel runs. In this case it is important to use a SLAR system in which the radar beam can be emitted from either side of the aircraft, so that the same 'look' direction can be maintained when the aircraft reverses its course after completing a run.

Stereoscopic SLAR coverage can be obtained by flying partly overlapping strips.

Two principal directions can be defined as shown in Figure 1: the along-track direction is parallel to the aircraft flight track, and the across-track (or range) direction is at right angles to it. The distance from the aerial to a ground object A is defined as the slant range of the object. The distance from the ground track of the aircraft to a ground object is called the ground range of that object.

The ground resolution of a SLAR system can be defined as the minimum spacing between ground reflectors which can cause independent echoes. The smallest area that can be resolved is called a resolution cell; its sides are the across-track resolution and the along-track resolution.

## ACROSS-TRACK RESOLUTION

In the across-track direction, returns start to come back from a reflector when the front of the pulse reaches it, and cannot be distinguished from any other return until the back of the pulse passes the reflector. Therefore the shorter the pulse, the finer is the across-track resolution. But the pulse duration cannot be reduced beyond certain limits: short pulses carry less energy than long pulses, thus their range is shorter. For ranges of about 20 km, pulses of about 10 microseconds would be required: with such a pulse, the across-track resolution would be about 2 km.

To obtain fine resolution without reducing the transmitted power, a method has been devised, called artificial pulse compression: the radar wave is modulated and only the high energy part of the modulated wave is used. In this way maximum slant ranges of over 50 km and across-track resolutions of about 15 m can be obtained.

## ALONG-TRACK RESOLUTION

Resolution in the along-track direction depends on the size of the aerial and on the method of recording and processing the radar returns. Two classes of SLAR systems can be identified: real-aperture or brute-force radars (e.g. Westinghouse AN/APQ-97) and synthetic-aperture or coherent radars (e.g. Goodyear GEMS 1000).

### Real-aperture systems

The real-aperture radar is very simple: the echoes from ground objects are received and processed into images without manipulations. Objects in the along-track direction produce separate echoes when they are spaced farther apart than the width of the radar beam. Thus narrow beams are required to produce a fine resolution.

Two factors play a role in controlling the beam width: wavelength and length of the aerial (aperture). The shorter the wavelength and the longer the aerial, the narrower is the beam. But if wavelengths shorter than several millimetres are used, the system starts losing one of its most important

characteristics, that of penetrating clouds and rain. And there is a limit to the size of aerial that can be carried by an aircraft. For these reasons, real-aperture radars generally have relatively poor resolution. A comparison between resolutions of different SLAR systems is shown in Table 1, page 6.

Synthetic-aperture systems

Synthetic-aperture radars are those in which a Doppler shift in the frequency of the received signal is used to obtain improved resolution: the actual aperture can be only a few metres, but the effective length that is achieved electronically is many times the actual aperture; hence the term 'synthetic'. The operation of these systems is outlined below. A complete description is given by Brown & Porcello (1969), and Grant et al., (1973).

As the SLAR-carrying aircraft moves forward, each reflecting target on the ground moves, relative to the aerial, across the beam in the along-track direction. During this movement the target is 'illuminated' several times by successive pulses, and each time it sends an echo back to the aerial. The relative movement of the target produces a change in the frequency of the reflected signals (Doppler shift), exactly in the same way as the note of the engine whistle changes when a train passes.

At a given instant, different targets at the same range, but separated in the along-track direction, have different and unique velocities with respect to the aerial. The history of frequency changes at that range contains the information needed to separate different targets.

The along-track resolution therefore depends on the possibility of detecting small frequency changes. This possibility is directly related to the quality of reception, in particular to the signal-to-noise ratio. Assuming no losses, the improvement of the signal-to-noise ratio is directly related to the number of returns from each target, that is, to the number of pulses transmitted while the target is in the area of the beam.

This number can be increased either by increasing the pulse repetition frequency (prf), or by increasing the beam width, or by decreasing the aircraft velocity. However: if more than one pulse is in flight across the imaged area at one time, the range determination will be ambiguous, hence the maximum prf is constrained by the pulse duration and by the range; increasing the beam width increases the 'illuminated' area and decreases the power per unit area; the velocity of the aircraft can be varied only within

certain limits and any decrease increases the mission cost. Therefore there are limits to the maximum along-track resolution obtainable by increasing the number of pulses.

However the resolution can be further improved by conveniently manipulating the reflected signals. As the wave returned by a reflector is spherical, whereas the aircraft path is nominally a straight line, there are small phase differences between the various echoes received from the same target. During the signal processing stage an allowance can be made for these phase differences, thus improving the capability of detecting small frequency changes due to the Doppler effect. Radars having this capability are called focused synthetic-aperture radars.

The calculated along-track resolutions for focused and unfocused systems are presented in Table 1, which is reproduced from Grant et al., 1973; the authors warn readers to 'treat the values with caution because the instability of the aircraft flight may prevent the realization of the full theoretical capability'.

TABLE 1 - ALONG-TRACK RESOLUTION OF SYSTEMS WITH 5 m APERTURE AT 10 km RANGE

| Wavelength (mm) | Along-track resolution | | |
|---|---|---|---|
| | Real aperture (m) | Unfocused synthetic aperture (m) | Focused synthetic aperture (m) |
| 8 | 16 | 9 | 4.5 |
| 30 | 60 | 18 | 4.5 |
| 300 | 600 | 54 | 4.5 |

## RECORDING

In real-aperture radars, generally no recording is required: as they are received on board, the signals returned to the aerial from ground objects can be processed into radar images which are recorded on film (page 7).

In synthetic-aperture and in some real-aperture systems, the signals are recorded on film (called film record or data film), or stored in computer core stores, for later processing. These records are two-dimensional plots of return data. The scale in the along-track direction is generally much

larger than that in the across-track direction. For example in the Goodyear system the scales are respectively 1:5550 and 1:400 000. This scale difference is then eliminated during processing.

## PROCESSING

### Real-aperture systems

In real-aperture radars the energy reflected from ground objects and returned to the aerial is converted by the receiver into a video signal (Fig. 2).

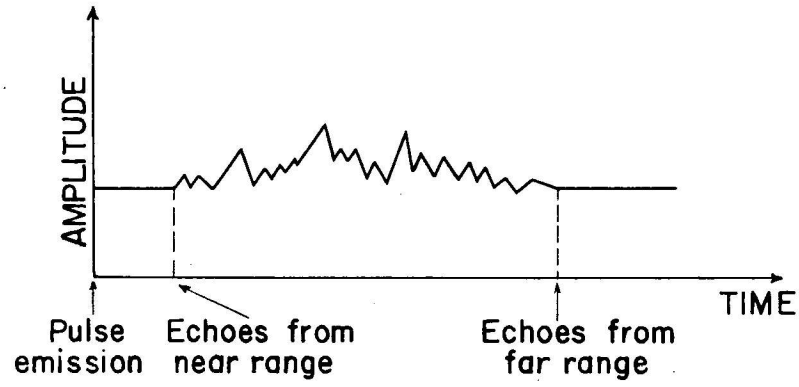


Fig. 2 - Amplitude of echoes from a single pulse

This signal is a function of the energy returned: the amplitude of the signal is directly proportional to the intensity of each echo; the time delay between the emission of a pulse and the reception of each echo is proportional to the distance between the aerial and the target which produced that echo.

This video signal is used to intensity modulate a cathode-ray tube (CRT); a sweep of the CRT beam across the display screen corresponds with the movement of a radar pulse from near to far range. The resulting line on the screen is a display of the radar image of the area 'illuminated' by that pulse. By means of an optical system the line display on the CRT is projected onto photographic film.

Returns from subsequent pulses are displayed on the same line of the CRT. By moving the photographic film in front of the CRT at a velocity proportional to the velocity of the aircraft, the radar image of the terrain is built up along the film. In the positive copy of the image, light tones correspond with high energy returns.

Synthetic-aperture systems

In synthetic-aperture systems, processing can be done in several ways; generally, the recorded signal is compared with the signal from an internal oscillator which produces a replica of the echo expected from a single ground reflector. In this way the system analyses the history of frequency changes at each range and separates the echoes of each target from those of the other targets. Then the echoes of each target are integrated to produce a video signal, similar to that produced by a real-aperture radar.

The display and recording of the radar image is done in the same way as for real-aperture radars.

## POLARIZATION

In most SLAR systems produced so far (e.g. Goodyear GEMS 1000) the aerial transmits and receives an horizontally polarized beam. Some instruments (e.g. Westinghouse AN/APQ-97) transmit a horizontally polarized beam and can receive both horizontally and vertically polarized beams (respectively called like-polarized and cross-polarized return).

Only a few experimental models (e.g. that of the University of Michigan) can both transmit and receive either type of beam.

## WAVELENGTH

The radar part of the em spectrum spans from 3 to 1000 mm in wavelength, or from $10^{11}$ to $3 \times 10^{8}$ Hz in frequency. This span has been divided into bands, designated by letters.

Table 2 shows the USA band designation and the wavelengths/ frequencies at which some SLAR systems operate. A different band designation is used in the UK and a still different one has been approved by NATO (Grant et al., 1973).

## TABLE 2 - RADAR BANDS AND SLAR SYSTEMS

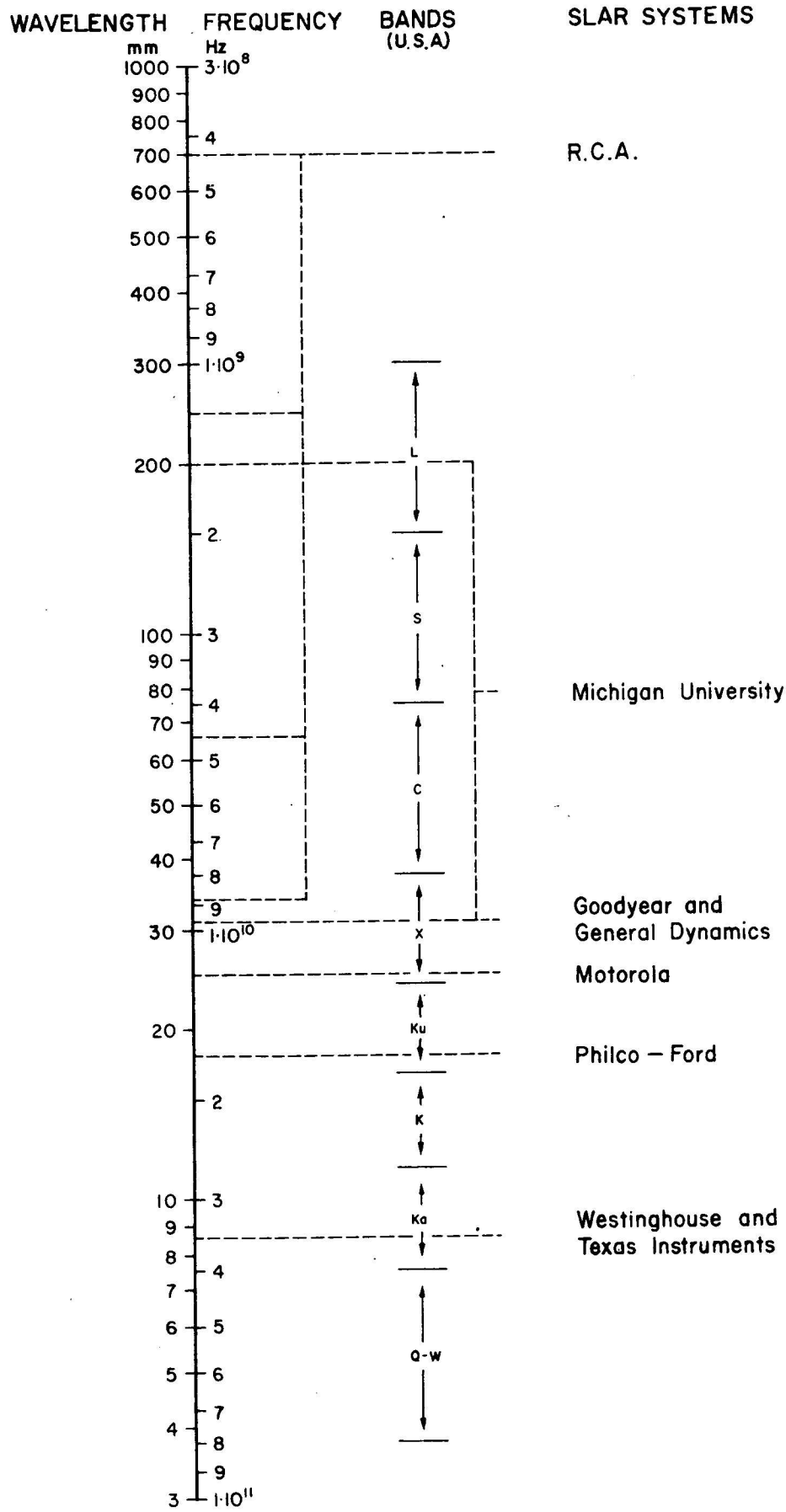


(re-drawn from GRANT et al. 1973)

## GEOMETRICAL ACCURACY

A common belief about SLAR is that, since the beam is oblique with respect to the horizon, the image produced is an oblique view of the terrain. This is wrong: distances between objects in the along-track direction are measured by means of the forward movement of the aircraft, which is constant; distances in the across-track direction are obtained during data processing by converting slant ranges into ground ranges, by means of an accurate knowledge of the height of the platform above the terrain. The resulting imagery is an orthogonal projection of terrain features.

Goodyear claim that the maximum inconsistency between scale along-track and scale across-track in their SLAR imagery is 1 percent. Staff members of the Radam Project (Brazil) tested the Goodyear imagery of the Amazon region and found it well within that specification (Van Roessel & De Godoy, 1974).

National Mapping personnel tested the planimetric accuracy of the Mt Isa SLAR mosaic by comparing it with 1:100 000 scale topographic maps (DNM, 1973). The co-ordinates of 28 identifiable points were derived from the mosaic and compared with those derived from the maps. The result was:

| | East | North |
|---|---|---|
| Largest difference | 300 m | 160 m |
| Least difference | 40 m | 20 m |
| Mean difference | 130 m | 90 m |

## SLAR MOSAICS

The geometrical accuracy of SLAR imagery assures good matching between contiguous strips having the same 'look' direction. Thus the strips can be easily joined together to make excellent mosaics. It is impossible to match strips that have been flown with opposite 'look' directions over hilly terrain.

The preparation of SLAR mosaics is often cheaper than that of good quality airphoto mosaics: the airphotos are conical projections and, unless the terrain is flat, it is often necessary to rectify them to obtain good matching.

From stereoscopic SLAR imagery, mosaics can be prepared by using every second strip. The remaining strips will then give stereo when viewed in combination with the mosaic.

## 3. RELATIONS BETWEEN SLAR IMAGERY AND TERRAIN FEATURES

The tonal variations on SLAR imagery represent changes in the amplitude of the radar terrain return. To interpret the imagery it is therefore important to know which parameters affect radar return, and what are their effects and interactions.

MacDonald & Waite (1973) list five parameters:

1) Surface roughness
2) Incidence angle
3) Dielectric contant
4) Frequency
5) Polarization

In the author's opinion, another parameter should be added to the list:

6) Look direction.

In addition it is very important for the interpreter to know the geometrical relationship between SLAR image and terrain, because this knowledge allows him to identify morphological features in the radar image.

The effects of each parameter and the possible geometrical deformations are summarized in the following discussion.

### PARAMETERS AFFECTING SLAR IMAGERY

#### Surface roughness

A surface is considered smooth in the radar sense when $h_m \leq \frac{1}{8} \lambda \cos\alpha$ , $h_m$ being the mean height of the irregularities of the surface, $\lambda$ the wavelength of the beam and $\alpha$ the angle of incidence (Macdonald & Waite, 1973, page 148). If $h_m \geq 2 \lambda \cos \alpha$ , the surface is considered rough.

Surfaces with intermediate values of $h_m$ are considered moderately rough.

For example, if $\lambda = 3.12$ cm (Goodyear GEMS 1000), a surface at near range ($\alpha = 45°$) is smooth when $h_m \leq 0.1$ cm and rough when $h_m \geq 1.6$ cm; a surface at far range ($\alpha = 75°$) is smooth when $h_m \leq 1.1$ cm and rough when $h_m \geq 4.4$ cm.

It can be seen from the above that the roughness is a function of wavelength and incidence angle: the same surface is smooth to long wavelength beams and rough to shorter wavelength beams; also a given surface appears smoother at large incidence angles (near grazing) than at small incidence angles.

When em energy is incident on a smooth surface, some of it may penetrate beyond the surface and be absorbed, but any that is not absorbed is reflected at an angle of reflection equal to the angle of incidence (Fig. 3a). If the surface is rough (Fig. 3c) the energy which is not absorbed is scattered

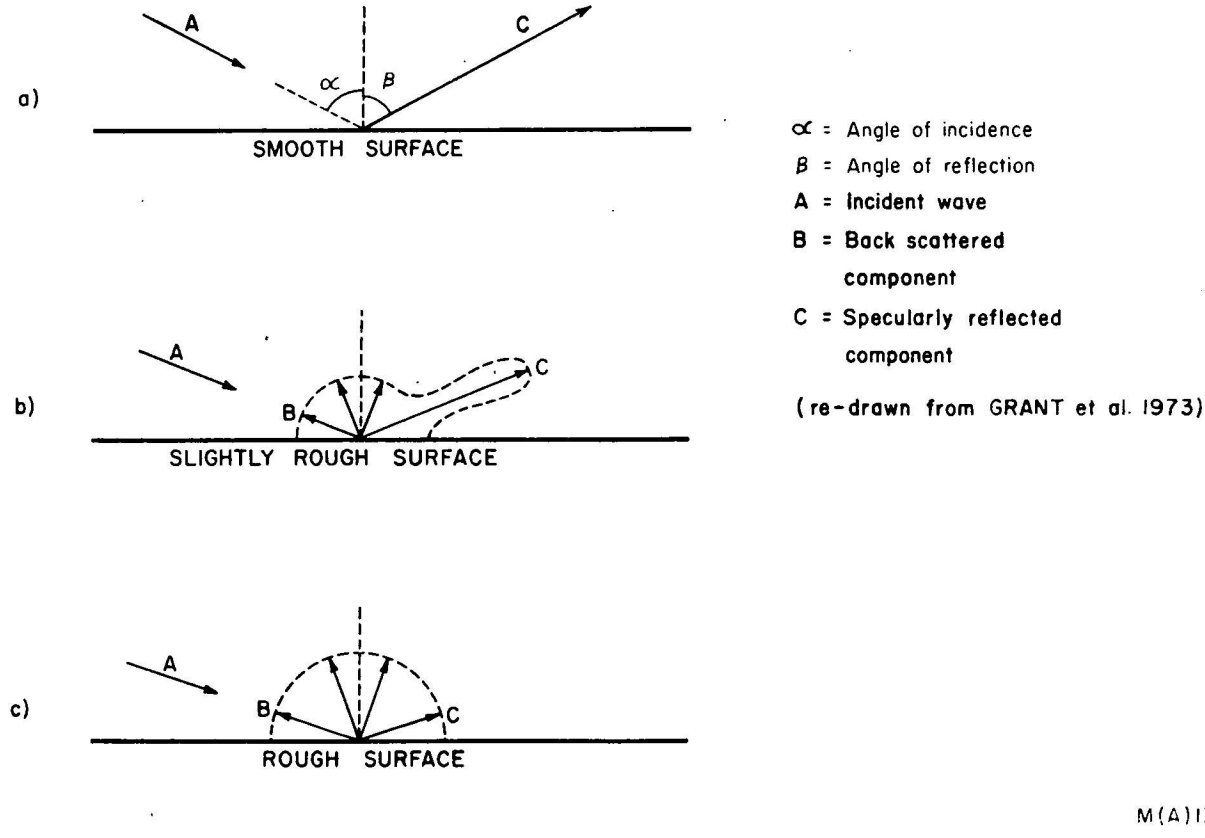


Fig. 3 - Scattering and reflection of radar energy (qualitative)

in all directions. Surfaces with intermediate roughnesses (Fig. 3b) scatter

a small amount of energy in all directions and more in the specular direction; the specularly reflected amount is inversely related to the degree of roughness.

The energy that is scattered back in the direction of the aerial is called the backscatter. Figure 3 indicates qualitatively, but not quantitatively, how the backscatter depends on the surface roughness.

Incidence angle

When the reflecting surface is smooth or slightly rough, the amount of energy returned to the aerial decreases with increasing angle of incidence (Fig. 4): if the beam is perpendicular to the surface ( $\alpha = 0$), the specularly reflected component coincides with the backscatter and the amount of energy returned to the aerial is maximum; at near-grazing angle ( $\alpha \approx 90^\circ$), a maximum amount of energy is reflected away from the aerial. Therefore the slopes facing towards the aerial give stronger echoes than those facing away from it.

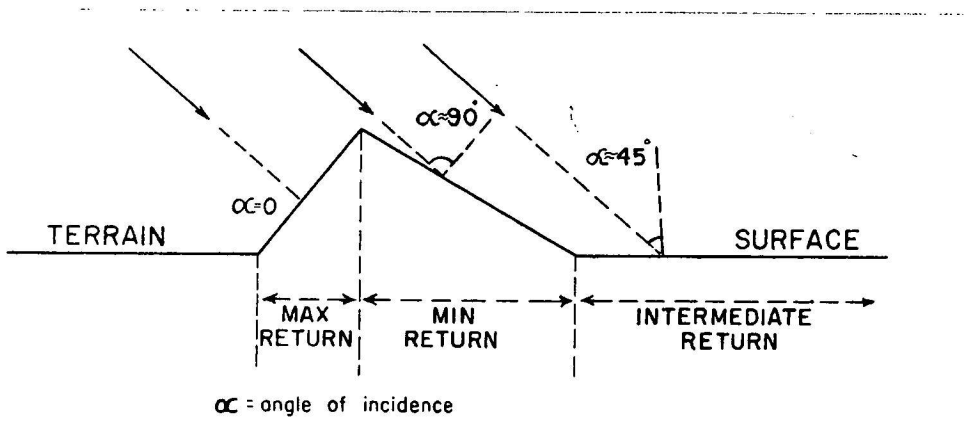


Fig. 4 - Radar return as a function of incidence angle

When the reflecting surface is very rough, energy is uniformly scattered in all directions, and the backscattered component is virtually independent of the angle of incidence.

If the surface forms a 90° corner reflector (Fig. 5), a specular reflection takes place regardless of the angle of incidence, provided that the beam lies in a plane perpendicular to the surface; this restriction

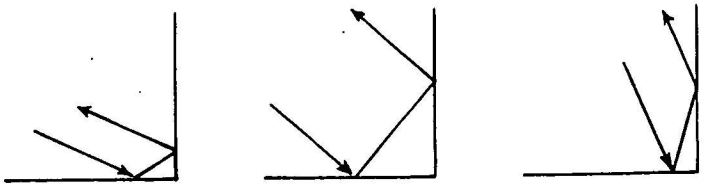

Fig. 5
Two-faced corner reflectors

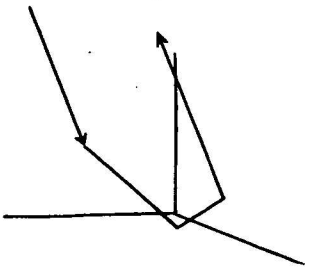

M(A)15

Fig. 6
Three-faced corner reflectors

does not exist if the surface forms a 3-faced corner reflector (Fig. 6). Natural corner reflectors are common on rocks with rectangular fracture patterns.

Dielectric constant

The higher the dielectric constant of the terrain surface, the higher is its microwave reflectivity. On natural surfaces the changes in dielectric properties are primarily due to changes in the water content. For example, wet soils are better reflectors than dry soils. Differences in the radar return from dense vegetation have been attributed to differences in the moisture content of the foliage (Macdonald & Waite, 1973, p.149V. Water bodies are very good reflectors but, at the angles of incidence used with SLAR, they are likely to reflect most or all of the energy away from the aerial.

The effect of the dielectric constant on radar returns is much weaker than that of surface roughness and of incidence angle; it can be observed and used as a diagnostic criterion only on fairly flat, smooth surfaces.

The dielectric constant is a function of the beam frequency; this relationship is discussed below.

Frequency

Roughness, dielectric constant, and penetration, hence the type and amount of information obtainable by means of SLAR, are related to the frequency of the beam.

A given surface appears rougher at high frequency (short wavelength) than at low frequency. Therefore high-frequency SLAR systems are likely to produce diffuse returns; low-frequency systems are more likely to produce specular reflections.

All materials have different dielectric constants at different frequencies. For example, the dielectric constant of water is zero at $10^8$ Hz, it rises to about 80 at frequencies in the X, Ku, K, and Ka bands, then it drops and becomes zero again at $10^{12}$ Hz. Since reflectivity is related to dielectric constant, which is related to frequency, then reflectivity is related to frequency. The best conditions for discriminating between targets are obtained when using the frequency at which those targets show the greatest possible differences in reflectivity. For example, both the Goodyear system (X-band) and the Westinghouse system (Ka-band) are suitable for the study of differences in the water content of natural materials.

The loss or attenuation of energy when a beam passes through a material controls the penetration of the beam. This loss is a function of the dielectric constant of the material, therefore a function of the frequency used. In general, the higher the frequency, the greater is the attenuation, hence the penetration is less. Experiments carried out at the Ohio State University (Macdonald & Waite, 1973, p. 149) show that X-band energy can penetrate a thin (13 mm) cover of vegetation, while Ka-band energy cannot. Vegetation penetration appears feasible with L-band radars (Waite & Macdonald, 1971). In sand or soil the water content controls the dielectric constant, hence the penetration of a given frequency. A table in Grant et al. (1973, p. 46) shows that the X-band penetration, calculated from dielectric constant measurements, is about 5 m for dry sand and about 10 mm for a soil containing 10 to 20 percent water.

To study the effects of frequency changes on radar imagery, experimental multi-frequency SLAR systems have been designed (Table 2). In the University of Michigan model the frequency cannot be changed automatically. In the RCA model the four frequencies can be changed automatically in sequence.

Polarization

If the terrain is very rough, the intensity of radar returns depends very little on the polarization planes of the beam. In fairly flat terrain there is a definite polarization dependency of radar returns. Several examples of this dependency are shown in Westinghouse (undated).

In general, images produced by means of cross-polarized beams (horizontal transmit, vertical receive) show good tonal contrasts between targets having different textures, such as alluvial materials having different grain sizes, or lava flows having different ages (hence, probably, different weathering and vegetation); forest non-forest boundaries and agricultural patterns can be better distinguished in images produced with like-polarized beams (horizontal transmit, horizontal receive). Like polarized beams are

little affected by target texture; hence they are best suited for the study of tonal contrasts which depend on other causes, such as incidence angle or dielectric properties of the terrain.

### Look direction

The amount of backscattered energy is generally greatest when the beam is perpendicular to the reflecting surface (Fig. 5). An obvious consequence is that SLAR imagery is directionally biased: structures (geological, agricultural, urban, etc.) perpendicular to the beam direction are imaged with good contrast; those parallel (in vertical view) to the beam direction may not be imaged at all. The interpreter who analyses structural features from SLAR imagery should take this bias into account. The problem can be avoided by flying perpendicular runs, but this would double the cost of the coverage, and increase the cost of the interpretation.

The look direction also controls the interpretability of relief in the imagery. SLAR imagery reproduces terrain relief as a succession of light and dark tones. The interpreter uses these tone differences to identify landforms. Therefore the interpretation of SLAR mosaics made from strips having the same look direction is easier than that of mosaics made from strips having different look directions. If the strips have opposite look directions, apparent relief inversions may occur (Fig. 8).

## GEOMETRICAL DEFORMATIONS

SLAR imagery is an orthogonal projection of the terrain, and its scale is fairly accurate. Nevertheless, it is not a perfect reproduction of terrain features. The main factors which limit the fidelity of the image are: poor resolution, radar shadow, and beam obliquity. Their effects are described below.

### Effects of poor resolution

Ground reflectors whose separation is smaller than the resolution are imaged as one reflector. Reflectors capable of originating strong returns can be imaged even if they are smaller than the resolution cell, but in the image they appear much bigger (for example, see the comment to Fig. 18).

Effects of radar shadow

The em radiation (Fig. 7) travels in straight lines and only objects which are visible from the aerial can be imaged. Behind these objects radar shadows, or areas of no energy return, are formed; these areas appear black in the imagery.

The length of radar shadow is a function of range: the longer the range, the longer the shadow. In Figure 7, object A produces an image A'; objects B and C are in shadow and cannot be imaged. The loss of information owing to radar shadow can be reduced by flying higher and increasing the depression angle. But to entirely cover very rugged terrain it is necessary to fly runs with various 'look' directions.

Even though radar shadows eliminate some terrain information, they are a valuable feature of SLAR imagery. They make small terrain undulations appear conspicuous and are the reason why SLAR emphasises the impression of relief. McAnerney (1966) describes a method for measuring terrain relief from radar shadow. Lewis & Waite (1973) have acquired quantitative geomorphic data by statistically analysing radar shadow frequencies.

Effects of beam obliquity (layover)

Figure 7 shows the types of geometrical deformations that occur when objects standing on an horizontal surface (datum plane) are imaged. Flight altitude and depression angles are the same as those used for the Mt Isa imagery; pyramids 1, 2 and 3 are 1500 m high.

Pyramid 1 is at near range, where the beam has a steep depression angle. The first echo from the pyramid is produced when a pulse reaches the top D. That echo could equally have come from point E, where the pulse intersects the datum plane; it is recorded on the data film as coming from a distance PD = PE, and the image of D, D', is closer to the near range than in reality. The same type of displacement affects all the points above the datum plane; the amount of displacement decreases with increasing range. The base line of the pyramid, FG, which is on the datum plane, does not appear to move and can be correctly positioned in the imagery. Face F'G'D', image of FGD, appears upside down: this phenomenon is called layover and occurs whenever the time sequence of the echoes is inverted because of terrain relief. Object H on the datum plane is imaged as if it was on face FGD. Echoes from faces DFI and DGL start arriving when face DFG is still reflecting, thus their images D'F'I' and D'G'L' will be partly superimposed on D'F'G'.

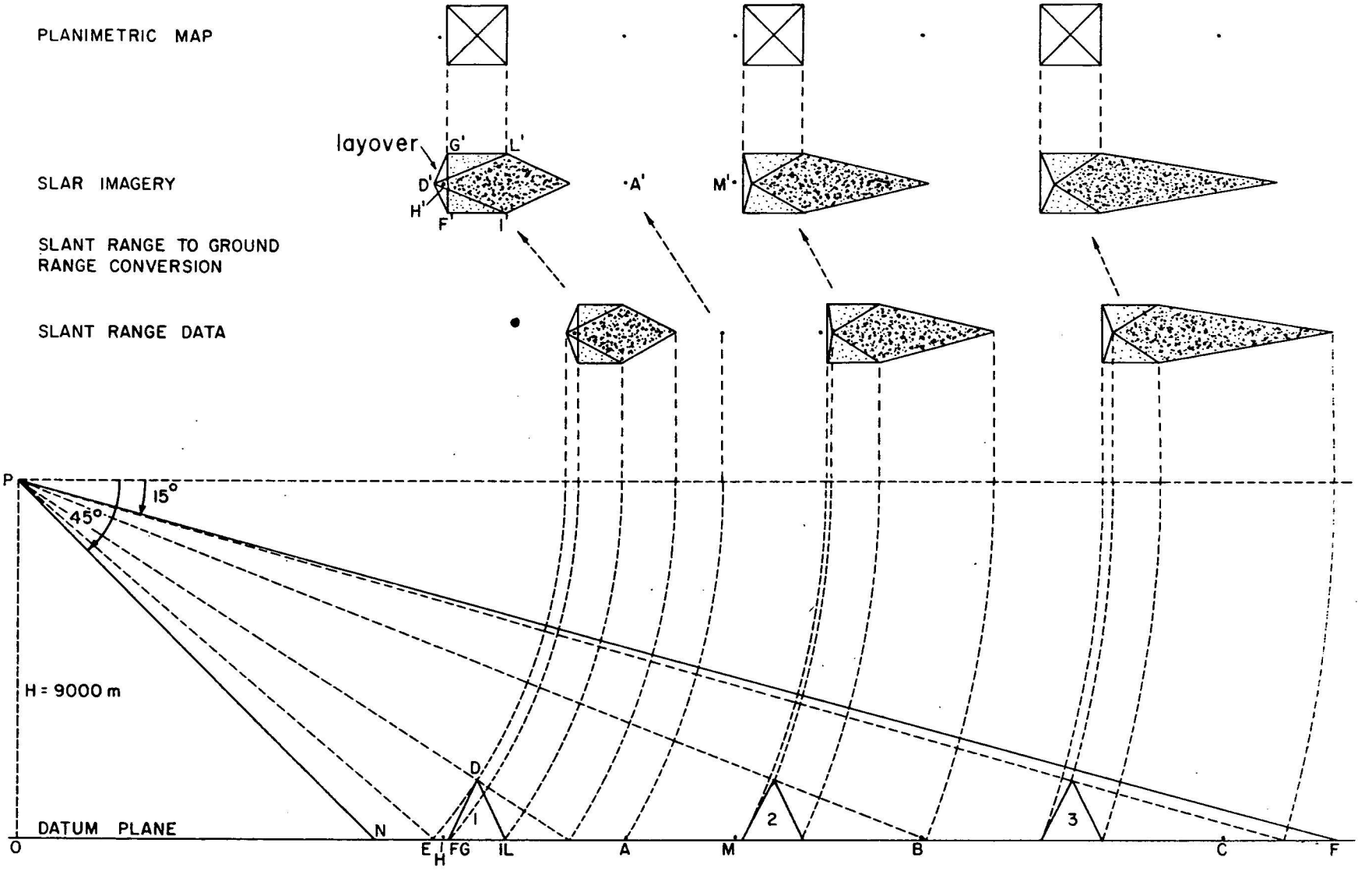


Fig 7—Geometrical deformations

As the pulse travels farther away from the aerial, the wavefront becomes steeper and layover is less likely to occur. Pyramid 2 is imaged as if leaning towards the near range, but no face appears overturned and the image of point M, M', appears in its correct position with respect to the pyramid. Pyramid 3, at far range, is the least deformed.

## 4. SLAR INTERPRETATION

### PROCEDURES

A systematic SLAR interpretation procedure is described by Barr & Miles (1970). The method was devised for the delineation of soil types by means of the identification of the parent material, and is applicable as well to other geological problems.

Very briefly it consists of:

a) Identification and delineation of 'pattern elements', by means of tone and texture observations (e.g. 'element with medium average areal tone, smooth texture').

b) Evaluation of 'patterns' formed by associations of pattern elements; the patterns are : patterns of drainage (e.g. 'dendritic, locally rectangular, very dense'); patterns of topography (e.g. 'hilly topography, moderate relief'); and patterns of land use (e.g. 'no evidence of agricultural activity; tone and texture indicative of brush and grass').

c) Inference of landform type (e.g.: 'bedrock hills').

d) Inference of geology (e.g.: 'consolidated sedimentary rock, possibly shale').

In Brazil, the Radam Project teams use a different method for the SLAR interpretation of the Amazon region. The imagery is interpreted for geology (lithology and structure), geomorphology, soil, and vegetation, with the purpose of preparing a map of the potential land uses. The lithological interpretation is based mainly on the analysis of drainage patterns; the structural interpretation mainly on the study of landform. The whole interpretation procedure is described in Maffi (1974).

Chapter 5 (page 31) contains a description of the procedure developed for the interpretation of the Mt Isa imagery.

Whatever method is used, the interpretation of SLAR imagery (as that of any other type of imagery) rests on the following basic principles:

a) Any two areas with the same rock type and geological history, under similar environmental and climatic conditions, should appear similar in the imagery.

b) Any two areas with dissimilar appearance, under similar environmental and climatic conditions, should have dissimilar rock type and/or geological history.

c) The interpreter is familiar with the imagery-terrain relations.

When these principles do not prevail, the interpretation is doubtful or impossible.

Some factors, such as fire, flood, and human actions tend to alter the appearance of natural objects, but a careful interpreter generally can identify these factors by means of their characteristic patterns.

The interpretation of SLAR imagery (as that of any other imagery) should be followed by a field check; a revision of the interpretation is generally necessary after the field check.

## EXAMPLES

This section contains the SLAR images of various geological and of some non-geological features, accompanied by brief comments. Half-tone printing has eliminated a considerable amount of fine detail; even so, these examples demonstrate the radar response of many different terrain features.

Some of the examples are of Papua New Guinea, and some of the Mt Isa area.

### Papua New Guinea examples

The imagery was flown in 1970 with Westinghouse equipment at a flight altitude of 6000 m above mean ground level. Figure 8. is a detail of the SLAR mosaic at 1:250 000 scale; the other examples are parts of SLAR strips at 1:220 000 scale. Unless otherwise indicated, north is towards the top of the pages.

Figure 8 - To some observers, the southern half may appear to have an inverted relief owing to 'illumination' from the south; to eliminate this effect, the interpreter should turn the page upside down.

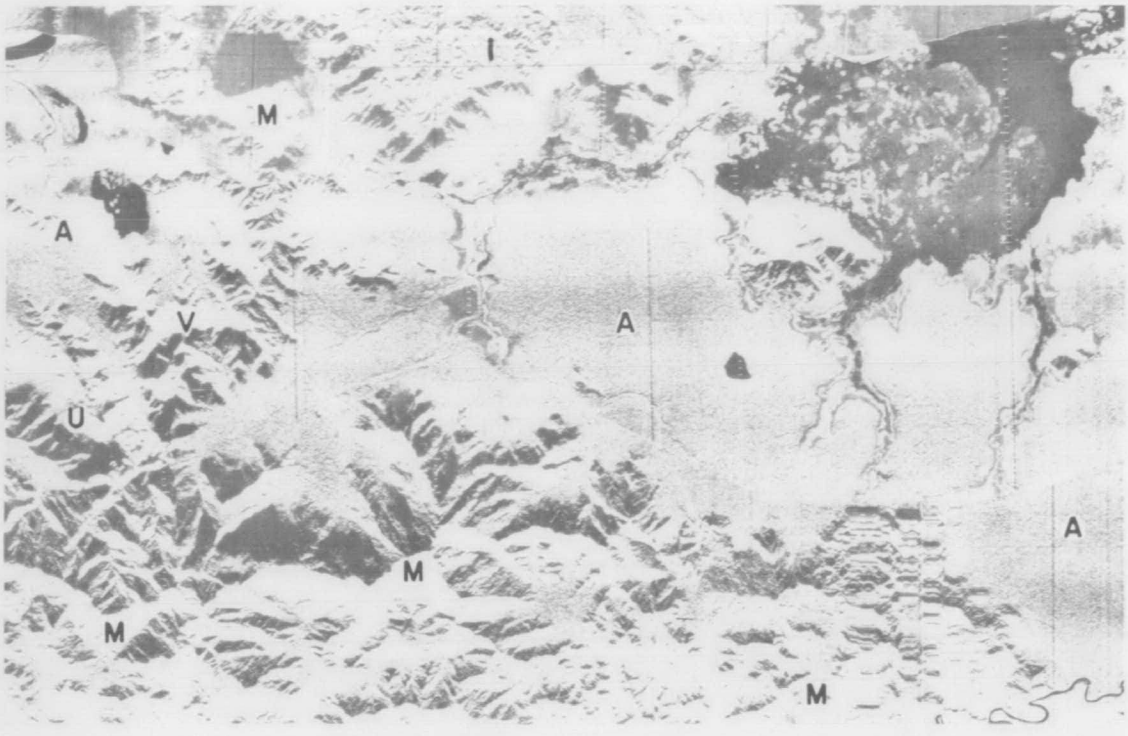


Fig. 8

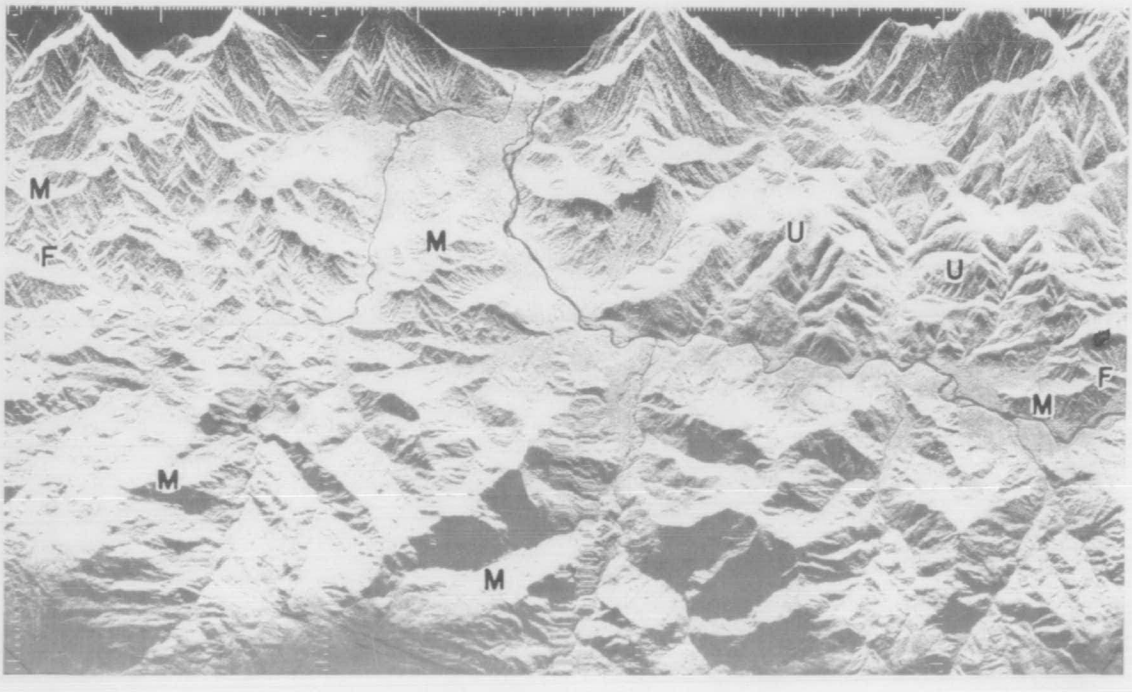


Fig. 9

A meander of the Sepik River appears in the northwestern corner. The dark area in the northeastern corner is Chambri Lake; calm water specularly reflects em energy away from the aerial and is imaged black; the dark grey areas with white patches are swamps. All other areas are covered by thick tropical forest. The flat, uniform, light to medium grey areas correspond to alluvium (A). Near the centre top, the low-relief area with a finely-speckled texture is occupied by intrusive rocks (I); two or possibly three sets of closely spaced fractures can be distinguished on I. The massive round-topped smooth hill at centre left is formed by ultramafic rocks (U) which, to the northeast, are faulted against volcanic rocks (V). All the other areas are underlain by metamorphic rocks (M).

Figure 9 - Layover is visible along the north side (Near Range). The Frieda Fault (FF) crosses the centre of the area roughly in an east-west direction. North of the fault, ultramafic rocks (U) form round-topped smooth hills and can be distinguished from metamorphic rocks (M).

Figure 10 - North is towards the bottom of the page. Oxbows and abandoned meanders fringe the Sepik River. A lake is visible near the centre top of the figure. The outcrops are formed by volcanic rocks. Though most of the region was cloud-covered during the SLAR mission, only a few heavy rainstorms, such as that near the top right corner, obscure the imagery.

Figure 11 - North is towards the bottom of the page. In this area near the estuary of the Fly River, tone differences allow the interpreter to separate blocked-valley swamps (as defined by Blake & Ollier, 191) from a dissected plateau (P). The swamps are imaged in light grey tones where they are covered by broad-leaf grasses, which reflect a fairly large amount of energy back to the aerial; and in dark tones where water predominantes. The plateau is imaged in medium to dark grey tones: the rainforest in this area behaves as a poor reflector. Note the corner reflector effect (bright reflections) along the slopes facing towards the top of the image (Near Range).

Figure 12 - North is towards the bottom of the page. The Lagaip River (lower left) and the Om River (lower centre) join together to form the Strickland River (centre). 1, 2, 3, and 4 are thrust sheets (as defined by A.G.I., 1962) of Tertiary limestone. The upper sheets form boat-like synclines, with Miocene siltstone in their cores. The thrust sheets partly overlie Mesozoic marine clastic sedimentary rocks. The correct interpretation of features like these would be impossible on imagery alone; but a limited amount of field information is generally sufficient to put the interpreter on the right track. Trend lines are clearly visible in many places in the Mesozoic rocks. Karst topography appears in some places on sheet 3 (centre left).

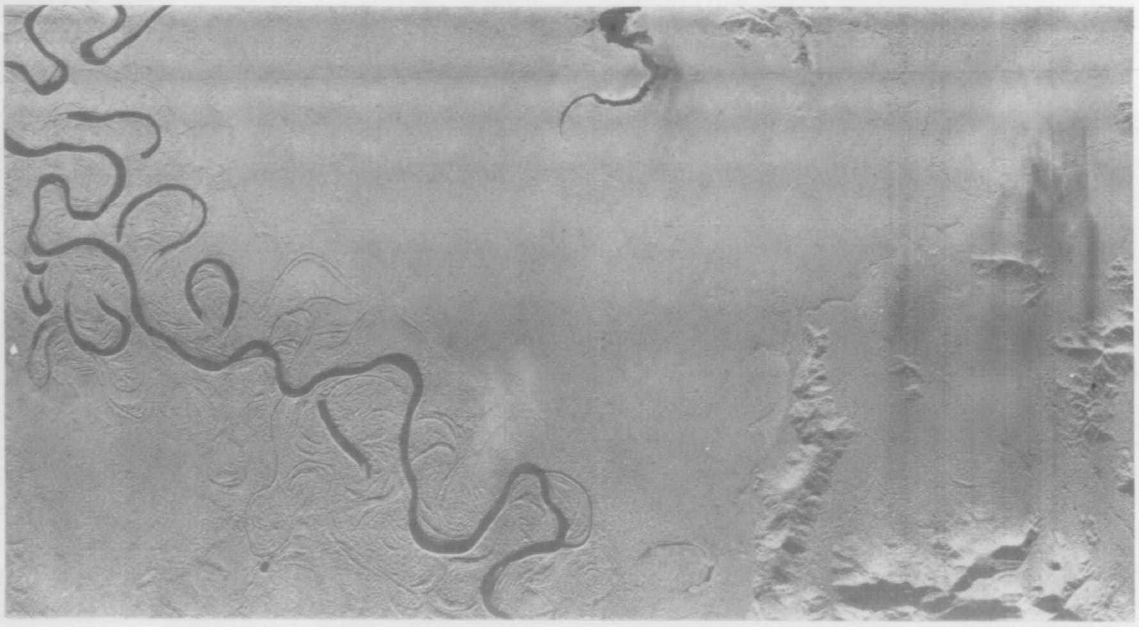

Fig. 10

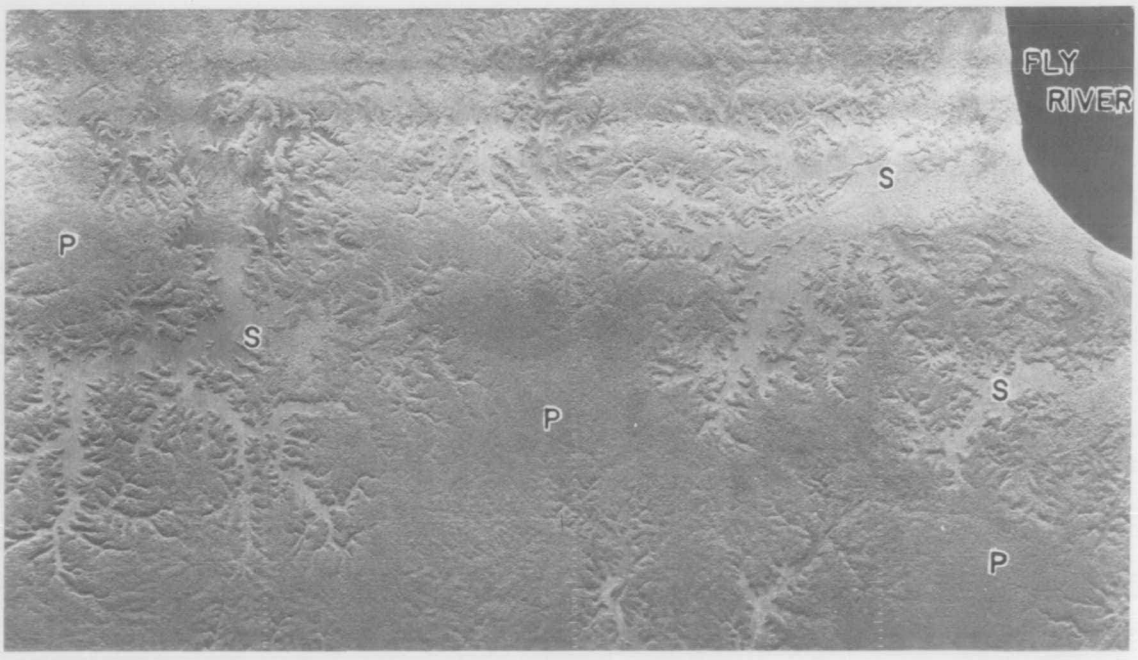


Fig. 11

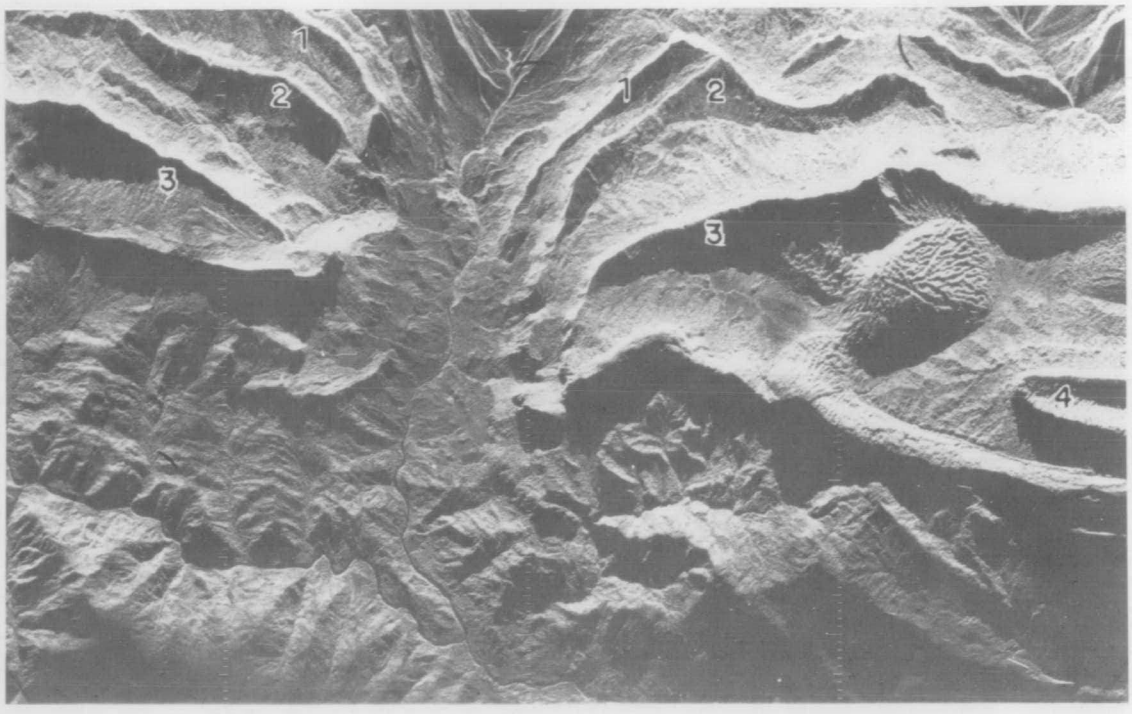


Fig. 12


Fig. 13

28

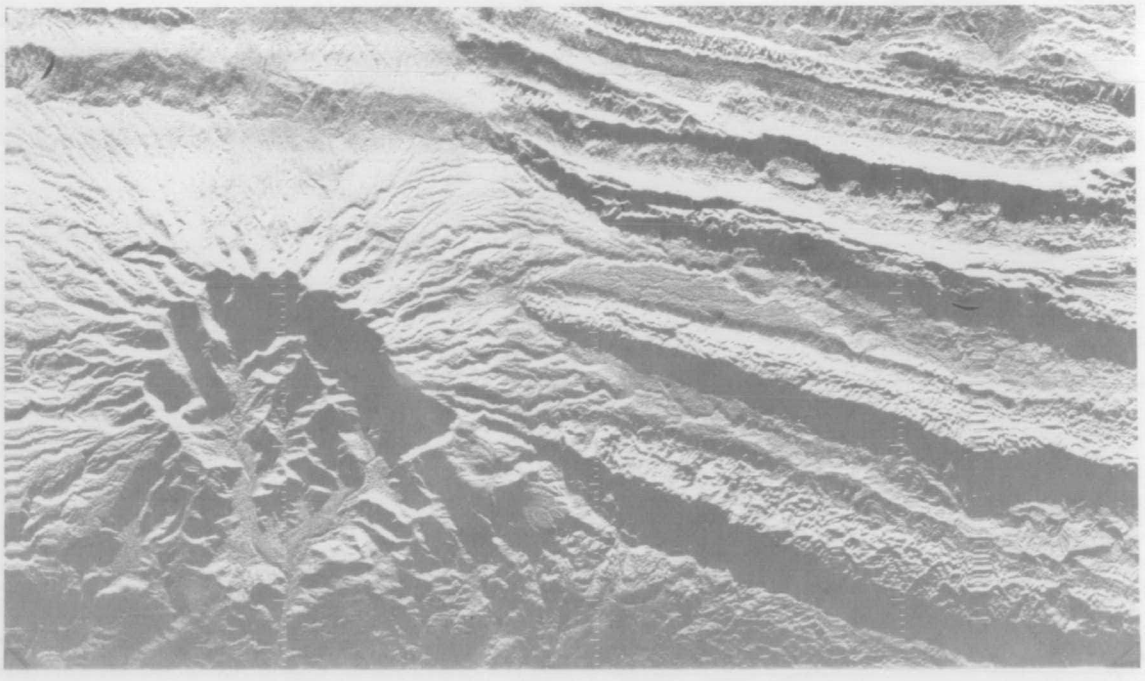

Fig. 14

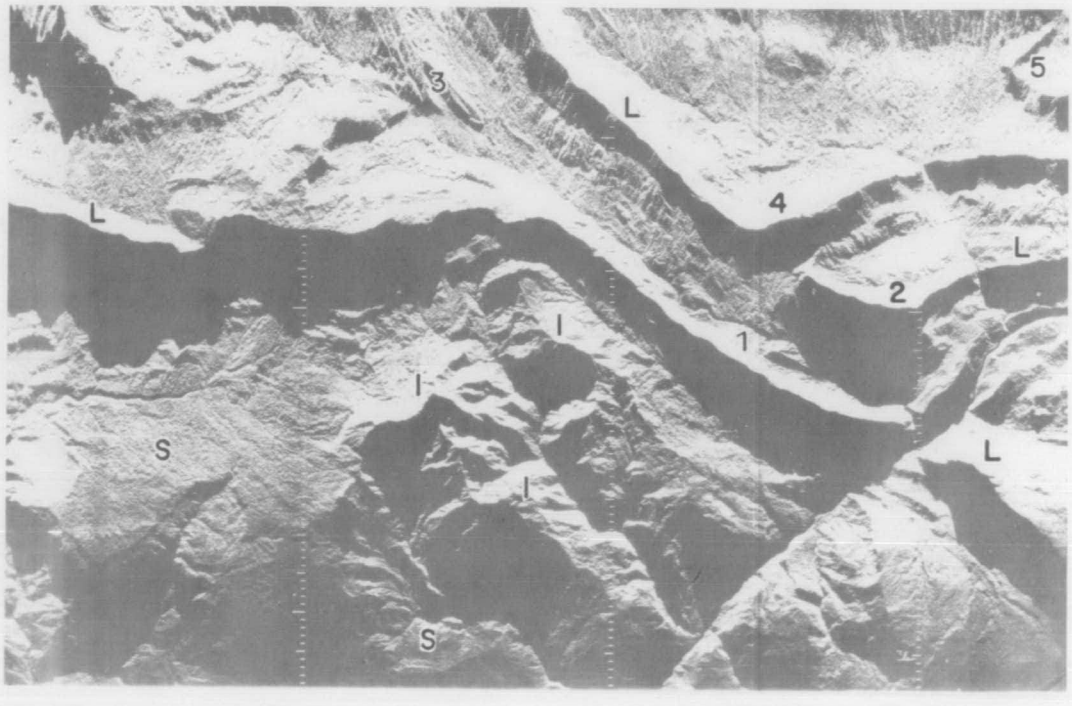


Fig. 15

29

Figure 13 - Before reaching the alluvial plains (lower left corner), the Strickland River crosses a series of synclines (S) and anticlines (A). The last crossed is the Cecilia Anticline, which is extremely well displayed in this image. In the northeastern corner of the figure Oligo-Miocene limestone crops out. Miocene and Pliocene marine and terrestial clastic rocks form well displayed dip-slopes.

Figure 14 - Eruptive products from a quarternary volcano, Mt Murray, overlie a sequence of thrust sheets formed by Tertiary limestone. The undulating, striped pattern of the lava flows is easily distinguishable from the spotted pattern of the karst topography, but the thrust-fault structure cannot be detected from the imagery alone.

Figure 15 - The narrow ridge across the centre of the image in a roughly east-west direction is the Victor Emanuel Range and the river in the southeastern corner is the Strickland. South of the centre, the massive-looking hills with a rectangular fracture pattern are formed by Upper Cainozoic diorite (I) intruding Mesozoic marine clastic sedimentary rocks (S). The northern half of the figure is occupied by Tertiary limestone (L). Limestone 1 is autochthonous; 2, 3, 4 and 5 are thrust sheets. Cretaceous shale and sandstone are visible between sheets 1 and 4. Folds and faults are visible in the limestone.

Mt Isa Examples

All the examples are part of SLAR mosaics of 1:100 000 scale. Information on the flight parameters is included in Chapter 5.

Figure 16 - The river crossing this area in a southwesterly direction is the Templeton River. A fault appears to have displaced its course; the river itself runs along a lineament, probably a fault. The interpretation is in Plate 1.

Figure 17 - This area is located a few kilometres north of Mt Isa. The medium grey, flat area marked Cz is occupied by Cainozoic deposits; isolated granite outcrops ($G_1$) are clearly visible. Granite occupies the fairly flat, dissected, fractured area $G_2$. The ranges to the east are formed mainly by quartzite and sandstone; the depressions between them mainly by shale and siltstone.

The Mt Isa Fault is difficult to map on SLAR particularly where it is parallel both to the bedding trend and to the radar beam: from A to B it follows the eastern side of a ridge; south of B most interpreters would probably trace it along the same side, to C; instead it crosses the ridge (BMR, 1973) and runs along its western side (B-D). The resulting inflexion is clearly visible on airphotos.

Fig. 16

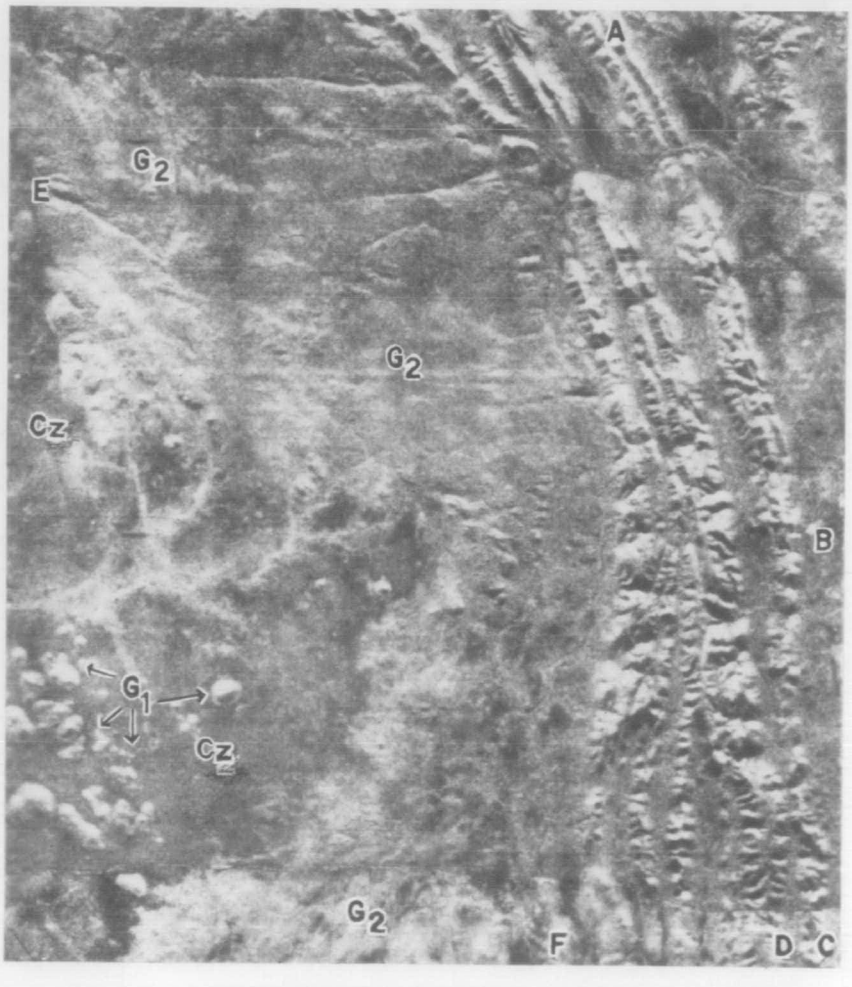


Fig. 17

Fault EF is un-mapped. On the SLAR mosaic it appears as a continuous, curved feature; on airphotos it appears formed by short straight faults.

Figure 18 - Near the northwestern corner, the dark, irregularly shaped patch is the vegetation clearing of Mt Isa airport: its flat smooth (in radar sense) surface reflects most of the em energy away from the aerial. The sealed north-south runway is not distinguishable in the clearing. The airport buildings are good corner reflectors and appear white. North of them, the metallic poles of a power line are perfectly visible, because of their high dielectric constant, even though their size is much smaller than the resolution; in the image they appear as if they were elliptically-shaped objects measuring 40 m in the along-track direction and 20 m in the across-track direction. Mt Isa town and several tailings dams are in the southwestern quarter.

The Mt Isa Fault (arrows) is visible with difficulty where it is parallel to the beam direction. Light-toned areas in relief are formed by quartzite and sandstone (Q). Among the flat areas, those imaged in dark tones are formed by siltstone and shale (S); those with a striped pattern are formed by predominantly volcanic rocks (V). Trend lines and light-toned quartzite lenses are visible in V. ff is a fault and jj a mosaic join.

Figure 19 - The white patch near the northwestern corner is Mary Kathleen town. G1, G2 and G3 are granite. G1 probably is weathered and soil-covered. Within G1, dark-toned linear features (aa, bb) are dolerite dykes, light-toned rounded hills (c) are remnants of dolerite dykes. Sedimentary rocks (mainly calcareous sandstone and quartzite), and slate and schist are marked S. A syncline is visible south of the centre of the figure. The linear feature dd has been mapped (BMR, 1972b) as a dolerite dyke; it is possible that similar features ee and ff are also dolerite dykes, though they have not been mapped. The Fountain Range Fault is indicated by arrows; its southern part, where it appears darker, coincides with the Northwestern Highway.

Figure 20 - The Cloncurry-Dobbyn railway (white line) and the Cloncurry-Quamby road (dark line) cross the Corella River. The tone difference is due to the difference in dielectric constants. The detectability of both railway and road depends on orientation relative to the beam direction, and an amount and height of flanking vegetation.

The flat areas with poor reflectivity are formed by Cainozoic deposits. The elongated outcrop with a transverse fault is formed by clastic sedimentary rocks (S); the irregularly shaped outcrops are formed by granite (G). In this and in other examples, most river beds are imaged in light tones; this means that their surfaces are rough in the radar sense (page 11).

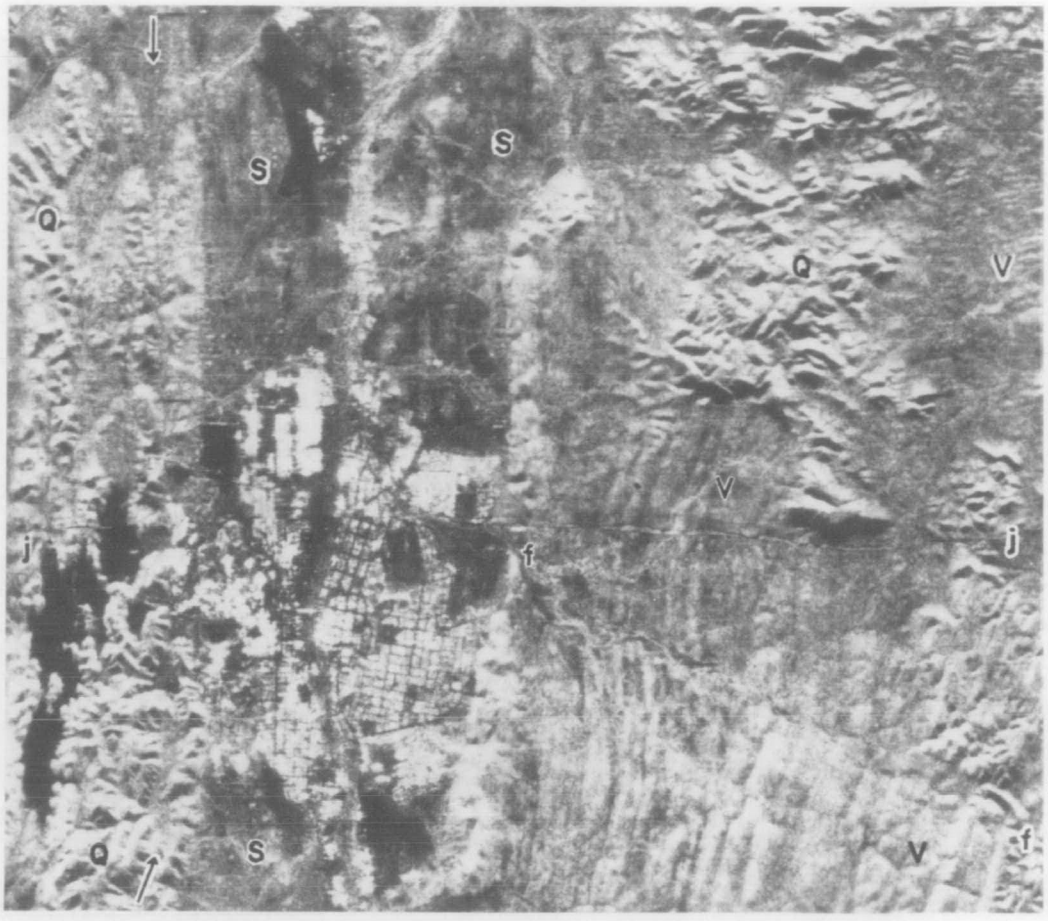


Fig. 18

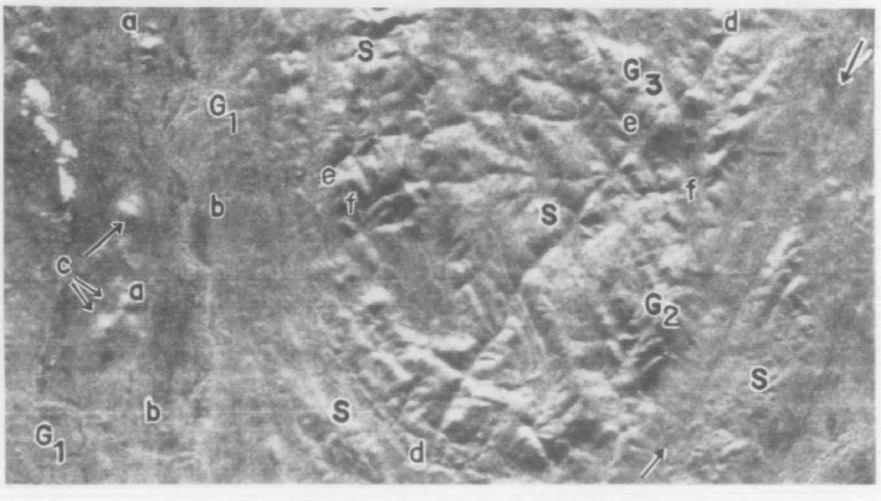


Fig. 19


Fig. 20

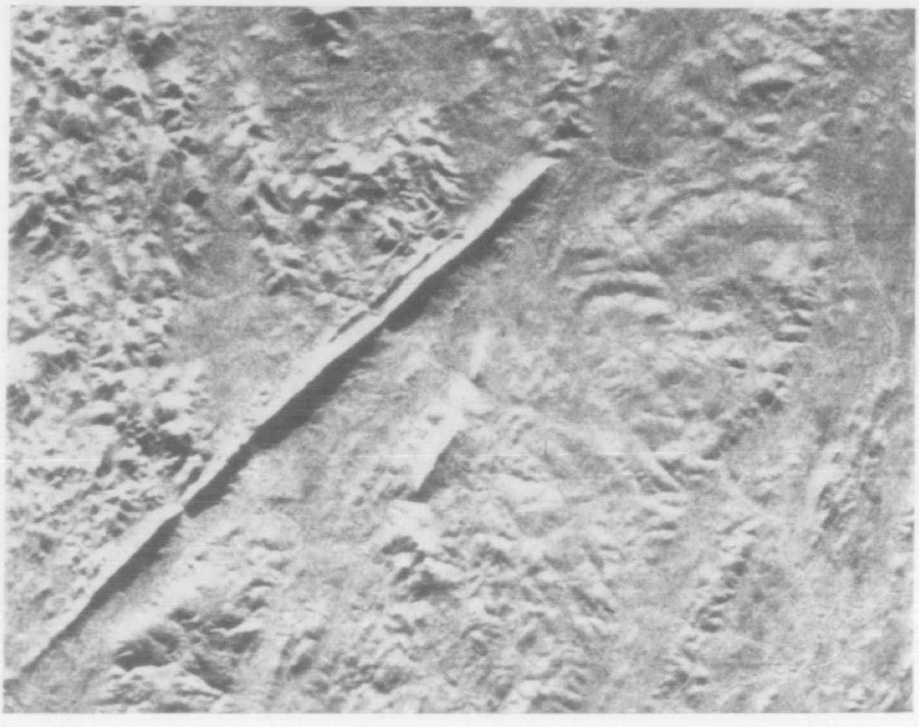

Fig. 21

Figure 21 - Fountain Range is a steep ridge formed by the quartzitic filling of the Fountain Range Fault. Maximum relief is about 200 m. On vertical aerial photographs this feature appears much less conspicuous.

Figure 22 - Ten km west of Malbon town, the corner-reflector effect reveals thin, low-dipping limestone beds of Middle Cambrian age. In the northwestern corner, the Camel Fault brings these beds into contact with Lower Proterozoic volcanic rocks.

Figure 23 - Along the Cloncurry River, about 40 km southwest of Cloncurry, tightly folded Proterozoic rocks crop out through Cainozoic deposits. By using tone and relief these rocks can be divided into quartzite (light-toned ridges) and interbedded volcanic rocks (dark-toned depressions).

Figure 24 - This area is about 65 km east of Duchess. The curving lineament ABCD is described on page 37.

Well displayed in the figure is also a syncline with north-northeast trending axis, formed by quartzite, slate, and schist. The fairly flat, fractured area in the northwestern corner is underlain by granite.

## 5. MT ISA SLAR PROJECT

In June 1972, the Division of National Mapping and BMR undertook a joint project for the evaluation of the mapping capabilities of SLAR in arid regions. The Mt Isa was selected because of the high economic interest and the availability of detailed ground information.

### The area

The region has an arid tropical climate; the annual rainfall ranges from 380 to 500 mm and is mostly limited to the four summer months December-March. The mean monthly temperature ranges from 31°C in January to 18°C in July.

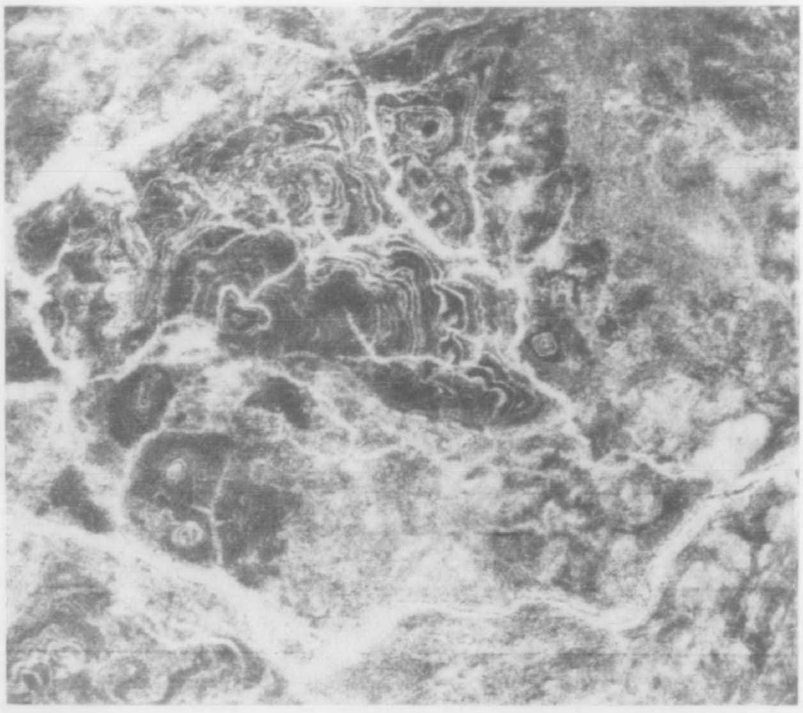

Fig. 22

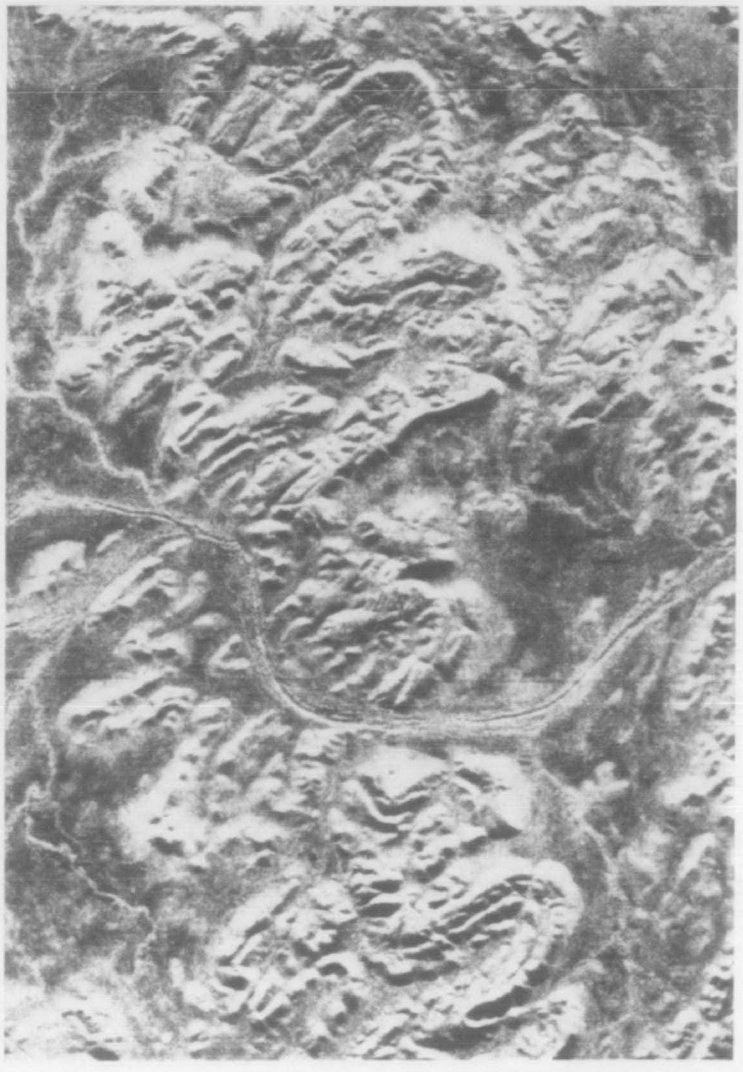

Fig. 23

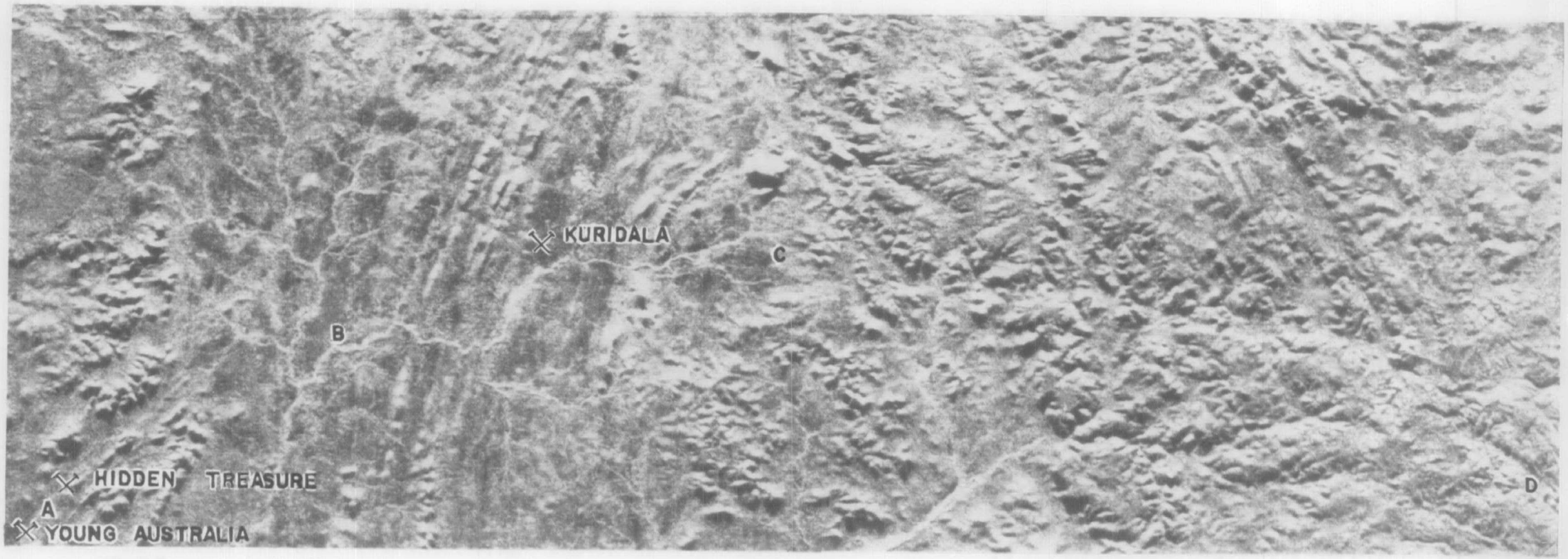


Fig 24



37

Except for a few flat tracts, the area is highly dissected; however, local relief exceeds 300 m in few places. The altitude above m.s.l. ranges from 200 m in the northeastern corner to about 650 m in the centre.

Large eucalypts thrive along the main watercourses. The plains are generally grassy and sparsely timbered. The hilly country supports light grasses, scrub, and low trees.

The airborne mission

The timing of the mission was chosen to take advantage of the movement from Indonesia to America of a SLAR-equipped aircraft; no such equipment is permanently available in Australia and mobilization costs from the USA would be prohibitive for a small project.

The cost of the coverage was $40 700, of which $20 700 were for flying and data collection, and $20 000 for mobilization to re-route the aircraft to Australia from the direct Indonesia-Brazil route.

Coverage of two areas was planned: area A (Fig. 25) is 100 x 30 km and was to be flown in east-west strips with radar looking south; area B is 30 x 15 km and was to be flown in north-south strips with radar looking west. On the day of flying, 17 June 1972, very strong high-level westerly winds were blowing. When flying in a driection perpendicular to the wind, the aircraft drift was greater than the antenna compensation capability, so the pilot decided to postpone the north-south runs to the next day. On 18 June the drift was still too great; the pilot abandoned the north-south runs and added a number of east-west runs to area A. A coverage much bigger than the 3450 $km^2$ stipulated in the contract was obtained and delivered to DNM/BMR at no extra cost: the mosaic covers about 15 000 $km^2$; the stereoscopic coverage is about 10 000 $km^2$.

Weather permitting, Super Wide Angle (SWA) and multi-spectral photographs were to be taken. On 1 June some colour IR photography was obtained before the weather deteriorated, but it is not usable because a blue filter had been left on the camera lens. On 18 June panchromatic photographs were taken soon after sunrise; the small sun-elevation angle produced shadows comparable with those of SLAR imagery. No multi-spectral photography was acquired because of the breakdown of the camera.

The flight parameters for the mission were:

Flight altitude: 9000 m a.g.l.
Near-range depression: 45°
Far-range depression: 15°

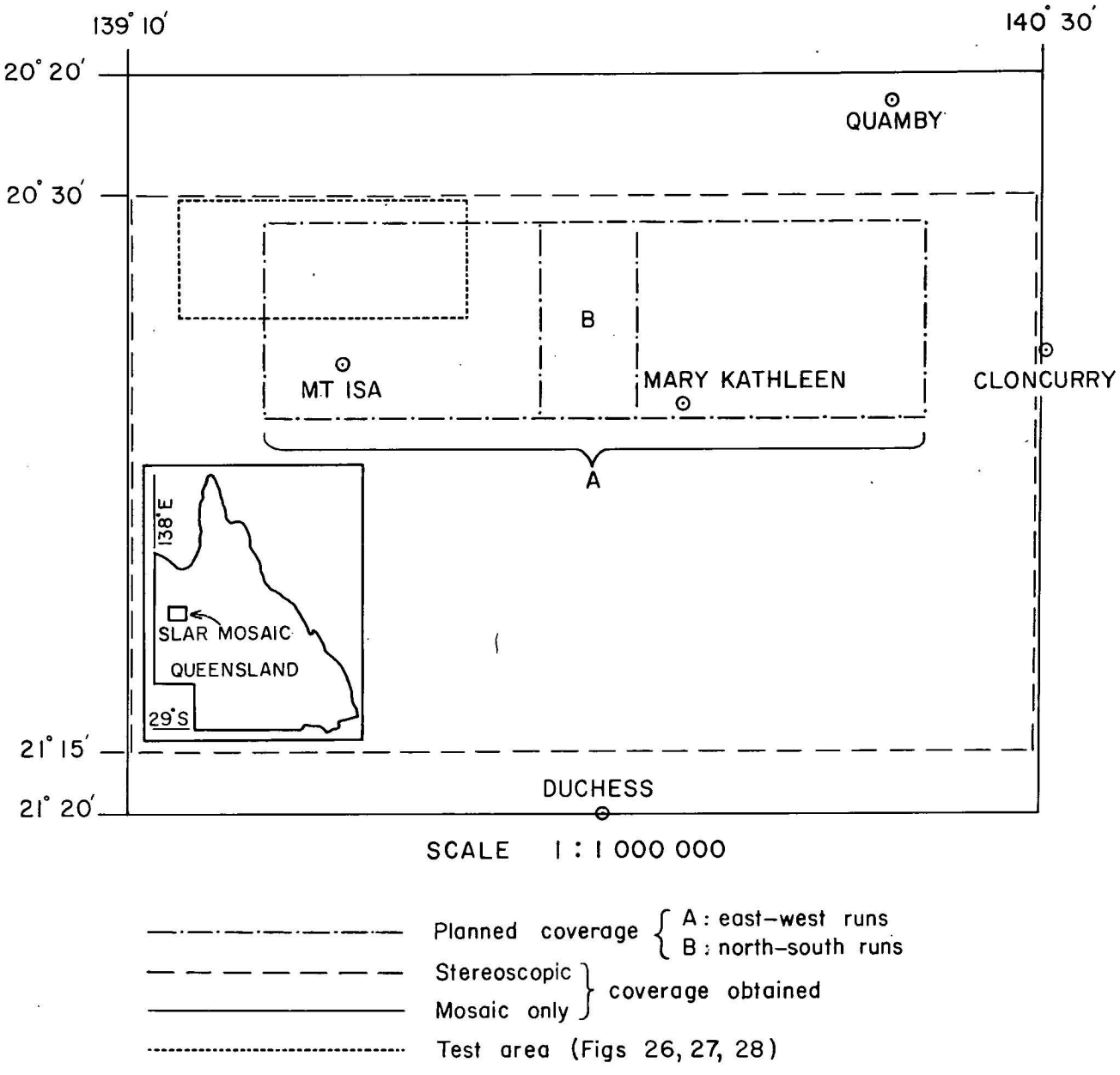


Fig 25 — MT ISA SLAR COVERAGE

Distance from aircraft ground track to near range: 9000 m
Distance from aircraft ground track to far range: 33 300 m
Maximum slant range: 34 500 m
Strip width: 24 300 m

The material supplied by the contractor (Canadian Aero Service Ltd) was:

A negative film at 1:400 000 scale of each SLAR strip
A negative film and a positive print of each SLAR mosaic at 1:100 000 scale (4 sheets)
A positive print of each 'stereo' strip at 1:100 000 scale (stereoscopic effect is obtained when viewing pairs formed by a 'stereo' strip and the mosaic)
Negatives and positives of all photography.

The equipment

The aircraft was a twin-jet Caravelle equipped with a Goodyear SLAR system model GEMS-1000, a Zeiss RMKA 8.5/23 camera and an $I^2S$ multi-spectral camera.

The specifications for the SLAR system were:

Type: focused synthetic aperture
Wavelength: 3.12 cm (X-Band)
Frequency: 9600 mHz
Antenna: one array on port side, one on starboard side, stabilized in roll, pitch and yaw. Either array coul be selected in flight
Polarization: horizontal transmit, horizontal receive
Beamwidth: horizontal 1.4°, vertical 45°
Resolution: 16 m along and across track at all distances
Pulse length: actual 0.9 microsecond; effective (after pulse compression) 0.06 microsecond.
Pulse repetition frequency: 1000 to 1600 pulses per second
Motion compensation of antenna: yaw $\pm$ 6°; pitch and roll $\pm$ 3°; drift $\pm$ 6° (this has been increased to 15° in recent models); look angle adjustment $\pm$ 17°.
Image scale: data film 1:400 000 in range, 1:5555 in azimuth; image film: 1:400 000 both dimensions
Nominal maximum slant range: 57.5 km
Maximum width of imageable swath: 37 km
Minimum far range depression: 10°
Maximum near range depression: 45°
Geometric fidelity achievable: 1% maximum inconsistency between scale along track and scale across track.

## INTERPRETATION METHOD

The interpretation was carried out entirely on 1:100 000 scale paper prints of the imagery, alternatively in monoscopic and in stereoscopic vision. The annotation, was made by means of colour pencils, on 0.075-mm thick Ultrapham sheets fixed to the northern edge of the mosaics in such a way that they could be easily lifted. This was necessary because both pencil marks and Ultrapham sheets tended to mask fine details in the mosaics.

The monoscopic study was made both with the naked eye and with a 1.5x self-supporting magnifying glass incorporated in an illuminator (Maggylamp, manufactured by Newbound & Co. Ltd).

For the stereoscopic study, a Toko mirror stereoscope equipped with a 3x binocular attachment was used; when the attachment is lifted off, a pair of 1.8x lenses can be inserted in the optical path to bring the image near the interpreter, so that the model appears to form at a distance of about 25 cm.

The following is a description of the interpretation procedure:

1. Preliminary interpretation:

   Annotation of linear features
   Annotation of drainage
   Identification and isolation of 'SLAR units', i.e. areas having uniform relief, drainage, tone, and texture
   Association of linear features and SLAR units with possible geological equivalents.

2. Check of preliminary interpretation against field information:

   Recently mapped 1:100 000 scale geological maps (BMR 1972 a, b; BMR, 1973; BMR, in prep.), which are the result of numerous traverses coupled with the interpretation of 1:25 000-scale colour aerial photographs, provided excellent field information. Therefore a direct field-check of the interpretation was unnecessary.

3. Final interpretation:

   Under normal circumstances, a SLAR survey would presumably be carried out where little or no geological information is available and the field check would be limited to a few traverses. To evaluate the Mt Isa imagery under similar circumstances, a test area of about 800 $km^2$ was selected on the mosaic and two hypothetical 'traverses' were traced across the test area; then, along these traverses, 'field' information from the geological maps was plotted; finally the test area was re-interpreted extrapolating from the 'traverses'.

To keep the evaluation of SLAR as objective as possible, the preliminary interpretation was carried out without reference to available ground data; however at that stage the interpreter already had some familiarity with the general geology of the area.

Plate 1 shows the preliminary interpretation (A), a lithological map produced from the 1:100 000 scale geological maps (B) and the final interpretation (C) of the test area.

## RESULTS

### Preliminary interpretation

a) Comparison of SLAR interpretation (Plate 1,A) with lithological map (Plate 1, B):

(SU = SLAR Unit; LT = Lithological Type).

SU1 generally corresponds with Cainozoic deposits (LT 1); in some places also with other lithological types (LT 2, 4, 6) where they crop out on flat terrain.

The boundary of SU2 matches very well with that of LT4 in the western part of the area. Because of the mesa-like relief associated with SU2 this unit was interpreted as formed by recent, poorly consolidated rocks; instead it is formed by Cambrian conglomerate, chert, and siliceous shale.

SU3 corresponds fairly well with LT3, both in rock type and in areal distribution.

SU4 in some places corresponds with LT3, in others with LT4. In others it has no analogy with any LT. It is formed by different rock types which produce similar radar signatures.

SU5 matches very well with LT5. Only one outcrop interpreted as SU5 is LT2. The geological equivalent of this unit, interpreted as soft sedimentary or low-grade metamorphic, is in fact metabasalt with minor interbedded tuff, quartzite, and sandstone.

SU6 is formed by intrusive rocks, as interpreted. Its distribution corresponds very well with that of LT6 where the rock forms large outcrops and shows characteristic fracture patterns, as in the northwestern part of Figure 17. Where the rock crops out from Cainozoic deposits (southwestern corner of Fig. 17) the boundaries can be readily trace even if the outcrops

are small and relief is low, because of the sharp tone contrast in the radar display; but rock type identification is uncertain and can only be estimated by analogy with large outcrops nearby. Where relief is low and fractures are not visible (e.g. western quarter of the area) or where small intrusive bodies occur among other rocks (e.g. northeastern corner), the correspondence between SU6 and LT6 is poor or nil.

SU7 has a distinct radar signature, but its composition and its air-photo signature are similar to that of SU3. A difference in surface roughness beyond the limit of airphoto resolution may be the reason.

b) Other features of the preliminary interpretation:

The main drainage can be easily delineated and matches fairly well with that of topographic maps at 1:100 000 scale; the differences are within the tolerance of the mosaic. The minor drainage channels can be easily mapped in fairly flat areas, but on rough terrain they can be mapped with confidence only under stereoscopic vision. The outline of several lakes on SLAR imagery is different from that on the topographic map (e.g. Lake Moondarra), owing to differences in water-levels in the reservoirs.

Many faults, lineaments, and sets of weathered joints have distinct radar signatures. Some, particularly those parallel to the beam direction (Fig. 18) are best detected under stereoscopic vision. The number of faults longer than 1 km in the preliminary interpretation is about the same as in BMR (1973) and BMR (in prep.). But faults shorter than 1 km are much more abundant in the geological maps than in the SLAR interpretation.

A fault and a lineament that have not been previously mapped are shown in Figure 16.

Several other lineaments are present in the area covered by the SLAR mosaic. One of the most interesting, because of its possible relation with copper mineralization, is the curving lineament ABCD in Figure 24, which has not been previously mapped in its full extent; part BC coincides with a dolerite dyke (Carter & Öpik, 1963). Because of its large size, the lineament is difficult to detect on aerial photographs; once detected, it can be followed fairly easily on RC9 photos at 1:85 000 scale, but with difficulty on K17 photos at 1:50 000 scale. On ERTS-1 imagery at 1:1 000 000 scale, it is visible where it is formed by large tone-contrasting elements not parallel to scan lines; the image in which it is best displayed is 1296-00081-5.

The lineament extends to the south and southeast beyond the limits of the SLAR coverage and is elliptically shaped, with a long axis of almost 35 km in the east-west direction and a short axis of about 27 km. The part of the lineament included in the SLAR coverage passes through two copper mines (Young Australia and Hidden Treasure) and very close to a third (Kuridala). To the south and southeast the lineament is less pronounced in areas of Mesozoic rocks, but there are several clues suggesting that it passes through Mt Elliott copper mine, south of Selwyn. If so, this lineament may be part of a structural feature related to copper mineralization in the area.

Bedding trends are generally easy to detect, particularly where they are not parallel to the beam direction. Where dip-slopes are present (Fig. 22) dips can be estimated under stereoscopic vision.

c) Comparison of preliminary interpretation (Plate 1,A) with 1:100 000 scale geological maps (BMR, 1973; BMR, in prep.):

The boundaries of the interpretation show much less detail than those of the geological maps.

Each SLAR unit includes several rock units (generally grouped by rock type).

Most of the major faults, many of the minor faults, and some unmapped lineaments are present in the interpretation.

In general, the preliminary interpretation is a much simpler (reconnaissance type) map than the 1:100 000 geological maps.

Final interpretation (Plate 1, C)

The final map shows known rock units instead of SLAR units; and more detail than the preliminary map.

There are many points of interest which deserve a comment. The following numbers correspond to the circled numbers in Plate 1,C. SI means SLAR interpretation (Plate 1,C). GM means geological map (either BMR, 1973; or BMR, in prep.). RC9 means Mt Isa/Cloncurry aerial photographs 4/96-110 and 5/64-76 at 1:85 000 scale, flown in October, 1966. Oc(s) means outcrop(s).

1 - Large oc of granite in GM, small scattered ocs of granite in SI. Probable reason for difference: granite is weathered and partly soil-covered.

2 - Small granite oc, not detected by radar.

3 - Previously unmapped lineaments, not visible on RC9 but clearly visible as tone alignments on SLAR.

4 - Previously unmapped lineament, clearly visible both on RC9 and SLAR.

5 - Oc of granite in GM, not visible on SLAR. Oc 5a, interpreted as granite, is instead Mesozoic capping.

6 - Previously unmapped lineament clearly visible on SLAR, partly on RC9.

7 - Fault in GM, not visible on SLAR nor on RC9.

8 - Previously unmapped fault, in RC9 appears formed by sequence of straight faults.

9 - SI and GM boundaries match very well.

10,11 - GM boundaries not visible on SLAR. SI is completely different from GM in this area. Possible reason : peneplanation has cancelled the effect of lithology on landform.

12 - Previously unmapped fault and lineament, both visible on SLAR and RC9.

13 - SI and GM boundaries match very well. North of 13, me and mi cannot be distinguished on SLAR.

Area between boundaries 13 and 9 - Granite ocs much smaller on SI than on GM. Probably same reason as at point 1.

14 - Previously unmapped fault well visible on SLAR and RC9.

15 - Fault on GM, perfectly visible on RC9, slightly on SLAR because parallel to beam direction.

16 - Boundaries not visible on SLAR, visible on RC9.

Area between 17 and 18 - Most GM boundaries can be recognised on SLAR, but not followed beyond 'traverse' zone. Shape and distribution of ocs in SI is very different from that in GM.

Area comprised within 18, 19, 20, 21 - all boundaries can be easily followed. SI agrees very well with GM. Exception : inflexion of Mt Isa Fault (see comment to Figure 17, page 25).

Area between fault 20-21 and boundary 22-23 - Pib is characterized by hilly landform, its boundary in GM agrees with that in SI. West of Pib, GM shows metabasalt (Phc, Phe), siltstone (Pin, Pik), and shale (Piu, Pig); they crop out in uniform, flat country and cannot be separated on SLAR.

Between 24 and 25 - No analogy between GM and SI.

Between 26 and 27 - Some analogy between GM and SI; better agreement can be observed between SI and BMR, 1972c. Southward, analogy decreases rapidly with increasing distance from 'traverse'.

Between 27 and 28 - Most boundaries and faults of GM match well with those of SI. Rock type differences are reflected by landform. Exceptions: dolerite 29 and dykes 31 and 32 cannot be detected on SLAR.

30 - Large oc interpreted as Phl for analogy with ocs along traverse A, is instead Phm, $Phg_1$ and $Phg_2$, whose rock type is similar to that of Phl.

33,34 - Faults, also visible on RC9, partly coincide and partly are aligned with faults mapped in GM.

Between 35 and 36 - Faults, boundaries and rock units of SI correspond with those of GM near 'traverse' zone; but starting from a distance of about 2 km north of 'traverse', similarity decreases rapidly. Beyond 3 km, only general shape of GM ocs is identifiable in SI.

The remarks on faults, lineaments, sets of joints and bedding trends made for the preliminary interpretation are valid also for the final interpretation. A quantitative comparision between faults in SI and in GM is shown in Table 3. The faults shorter than 1 km are difficult to detect on SLAR imagery; but if this class is excluded from the computation, the number of faults in SI is the same as the number of faults in GM. In the 5-10 km class, several GM faults are parallel to the direction of the radar beam and others are curvilinear: this resulted in poor detectability on SLAR imagery. In the class over 10 km, the number of SI faults is almost twice that of GM faults, a direct result of the synoptic view of the terrain offered by SLAR.

TABLE 3 - NUMBER OF SLAR-INTERPRETED VERSUS FIELD-MAPPED AND PHOTOINTERPRETED FAULTS IN TEST AREA

| Length classes (km) | Faults on SLAR interpretation (No.) | Faults on 1:100 000 map (No.) |
|---|---|---|
| Less than 1.0 | 16 | 102 |
| 1.0 - 2.5 | 90 | 89 |
| 2.5 - 5.0 | 38 | 30 |
| 5.0 - 10.0 | 9 | 21 |
| More than 10.0 | 7 | 4 |
| All faults | 160 | 246 |
| Faults >1 km long | 144 | 144 |

Comparison of SLAR imagery with simultaneous photography.

The colour IR photography taken on 17 June is not usable as such because of the blue hue. However two important facts emerge : a) few frames are cloud-free, and b) the coverage had to be abandoned when the weather deteriorated, while the SLAR mission continued unaffected.

The five runs of panchromatic photography taken on 18 June are practically cloud-free.

Run 1 and part of run 2 were flown too early in the morning and are affected by mist and long shadows.

Half of run 2, run 3, and about half of run 4 show no mist and the shadows are comparable with those produced by SLAR. As does SLAR imagery, these photographs emphasize the effect of relief, and therefore improve the interpretability of landforms. Their grey tones seem to be more closely related to lithology than those of SLAR imagery. Their resolution is much higher than that of SLAR imagery, thus they contain more information than SLAR imagery on rainage, vegetation, and man-made features.

Starting from about the middle of run 4, the low sun-angle effect begins to fade out. From the flight log prepared by the pilot, it can be seen that, on 18 June, photography with satisfactory low sun-angle effect was taken between 0730 and 0830 hours.

## CONCLUSIONS

The following remarks are valid for X-band SLAR imagery, when scale, flight parameters, and area are similar to those described at the beginning of Chapter 5.

The study confirmed for the Mt Isa area the well known properties of SLAR, described by many authors for other areas : all-weather capability, uniformity of illumination direction, emphasis on effect of relief, synoptic view of terrain, and suitability for reconnaissance geological mapping.

In several places different lithological types give similar radar signatures (e.g. SLAR Unit 4 is formed by lithological types 3, 4, and, to a lesser extent, 5 and 6). In some places similar lithological types give different radar signatures (e.g. lithological type 3 corresponds with SLAR units 3, 4, and 7). Some rock units can be easily outlined but their lithological type is difficult or impossible to ascertain (e.g. $\epsilon$me-$\epsilon$mi, Plate 1, C). However, in general, there is a fairly good agreement between SLAR interpretation and the lithological map at 1:100 000 scale : quartzite and sandstone can be identified mainly by landform, volcanic rocks by pattern, and intrusive rocks by fracture traces, where they are not deeply weathered and soil-covered. Calcareous rocks, shale, and siltstone are the most difficult to interpret.

The main interpretation tools are: the study of landform on hilly terrain; and the study of tone differences on flat terrain.

Structural features such as bedding trends, faults longer than 1 km, lineaments, and joint sets are well displayed. However there is a bias against linear features parallel to the radar beam direction; this should be taken into account particularly when carrying out statistical analyses of such features.

In structural interpretation SLAR imagery is particularly suitable :

a) For the detection of features ranging in size between 20 and 50 km, that is too large to be perceived on aerial photographs at usual scales (1:50 000 and 1:85 000), and too small to be readily identified on satellite images. After detection on SLAR these features can generally be recognized on aerial photographs or satellite images.

b) For the detection of features that are not displayed by aerial photography, such as some tone alignments in flat areas, probably produced by differences in dielectric contrast or in roughness (in radar sense) of ther terrain.

Of several new lineaments discovered on SLAR imagery, one may be connected with the presence of copper mineralization and should be further investigated.

The main drainage channels can be easily mapped from SLAR mosaics. Minor watercourses can be traced monoscopically with confidence only in flat areas.

Stereoscopic vision is not as necessary to SLAR interpretation as to photo interpretation. It helps in the annotation of minor drainage (particularly in hilly areas), in the annotation of linear features, and in the study of landforms; it allows the interpreter to estimate dips and to distinguish tonal differences due to relief from those due to other causes, such as dielectric constant or roughness of the terrain.

Where different rock types are accompanied by different morphological features and structure is very simple, such as in the ranges west of Mt Isa, traverses separated by as much as 10 to 15 km should be sufficient to check the preliminary SLAR interpretation. Where the geology is complex, closer traverses should be made. Traverses 2 to 3 km apart should be made to check the preliminary interpretation of areas as complicated as that to the southeast of Lake Moondarra. After such a field check, the final interpretation should provide valuable information for the planning and execution of detailed geological field mapping.

SLAR imagery should be considered as a complement, not as a substitute, for aerial photography.

Shadow effects similar to those of SLAR imagery can be obtained with low sun-angle photography, but owing to the rapid change in sun elevation, the useful flying time is about one hour a day; if illumination from opposite directions is not a problem, that time can be extended to one hour in the morning and one hour after noon. Therefore low sun-angle photography costs much more than normal photography.

The cost of SLAR coverage in Australia is very high. In 1972 it ranged between $\$6/km^2$ for an area of a few thousand square kilometres, to about $\$3/km^2$ for areas bigger than 50 000 $km^2$, in addition to aircraft mobilization expenses. A comparison between the cost of SLAR imagery and that of other types of coverage woul be misleading because other

remote sensors do not possess some of the SLAR properties mentioned above. Therefore the question whether SLAR is cost-effective in Australian semi-arid environments cannot be answered absolutely: the answer depends on the importance that some properties of SLAR may have for the solution of the particular problem being considered. These properties are: the combination of relief enhancement with synoptic view of the terrain, and the capability of defecting linear features that would be difficult or impossible to detect on aerial photographs or on satellite images.

## 6. REFERENCES

### WORKS CITED IN TEXT

A.G.I. (AMERICAN GEOLOGICAL INSTITUTE), 1962 - Dictionary of geological terms. Dolphin Books.

ANDERSON, V.H., 1966 - High altitude side-looking radar images of sea ice in the Arctic. Proc. 4th Symp. Remote Sensing of Environment, Univ. Michigan, Ann Arbor, 845-59.

BARR, D.J. and MILES, R.D., 1970 - SLAR imagery and site location. Photogramm. Engg, 36(11), 1155-70.

BLAKE, D.H., & OLLIER, C.D., 1971 - Alluvial plains of the Fly River, Papua. Z. Geomorph, Suppl. 12, 1-17.

BMR, 1972a - Cloncurry, Qld - 1:100 000 Geological Map, Sheet 7056, Preliminary Edition - Bur. Miner. Resour. Aust. (unpubl.).

BMR, 1972b - Marraba,Qld - 1:100 000 Geological Map, Sheet 6956, Preliminary Edition - Bur. Miner. Resour. Aust. (unpubl.).

BMR, 1972c - Mary Kathleen, Qld - 1:100 000 Geological Map, Sheet 6856, Preliminary Edition - Bur. Miner. Resour. Aust. (unpubl.).

BMR, 1973 - Mount Isa, Qld - 1:100 000 Geological Map, Sheet 6756, Preliminary Edition, - Bur. Miner. Resour. Aust. (unpubl.).

BMR, in prep. - Mary Kathleen, Qld - 1:100 000 Geological Map, Coloured Edition - Bur. Miner. Resour. Aust. (unpubl.).

BROWN, W.M., & PORCELLO, L.J., 1969 - An introduction to synthetic aperture radar. IEEE Spectrum, 6(9), 52-62.

CARTER, E.K., & ÖPIK, A.A., 1963 - Duchess, Qld - 4-mile Geological Series. Bur. Miner. Resour. Aust. Explan. Notes 23

DNM, 1973 - Side-looking airborne radar survey. Rep. to 7th UN Regional cartogr. Conf. Asia Far East, Tokyo, 15-27 October 1973.

GRANT, K. (group leader) et al., 1973 - Side-looking radar systems and their potential applications to earth resources surveys - European Space Res. Org. ESRO CR-141. (unpubl.).

LEIGHTY, R.D., 1966 - Terrain information from high altitude side-looking radar imagery of an arctic area. Proc. 4th Symp. Remote Sensing of Environment, Univ. Michigan, Ann Arbor, 575-97.

LEWIS, A.J., & WAITE, W.P., 1973 - Radar shadow frequency. Photogramm. Engg, 39(2), 189-96.

McANERNEY, J.M., 1966 - Terrain interpretation from radar imagery. Proc. 4th Symp. Remote Sensing of Environment, Univ. Michigan, Ann Arbor, 731-50.

MACDONALD, H.C., & WAITE, W.P., 1973 - Imaging radars provide terrain texture and roughness parameters in semi-arid environments - Mod. Geol., 4, 145-58.

MAFFI, C., 1974 - Remote sensing study in France and Brazil. Report on overseas visit August - December 1973. Bur. Miner. Resour. Aust. Rec. 1974/46 (unpubl.).

ROUSE, J.W. jr., MACDONALD, H.C., & WAITE, W.P.,1969 - Geoscience applications of radar sensors. IEEE Trans. Geosci. Electronics, GE-7, 1, 2-19.

VAN ROESSEL, J.W., & DE GODOY, R.C., 1974 - SLAR mosaics for Project RADAM - Photogramm. Engg, 40(5), 583-95.

WAITE, W.P., and MACDONALD, H.C., 1971 - Vegetation penetration with K-band imaging radars - IEEE Trans. Geosci. Electronics, GE-9, 147-55.

WESTINGHOUSE, undated - Side look radar (unpubl.).

OTHER WORKS

BEATTY, F.D., BECCASIO, A.D., BECKER, E.S., & BRADIE, R.A., 1967 - Geoscience potentials of side-looking radar. Raytheon Co. Rep. N. 67-33091, 2 Vol.

CAMERON, H.L., 1965 - Radar as a surveying instrument in hydrology and geology. Proc. 3rd Symp. Remote Sensing of Environment, Univ. Michigan, Ann Arbor, 441-53.

CLARK, M.M., 1971 - Comparison of SLAR images and small-scale low-sun aerial photographs. Geol. Soc. Amer. Bull. 82(6), 1735-42.

COLWELL, R.N. (chairman), 1963 - Basic matter and energy relationship involved in remote reconnaissance - Report of Subcommittee I, Photo Interpretation Committee, American Society of Photogrammetry - Photogramm. Engg, 29(5), 761-99.

CRANDALL, C.J. 1969 - Radar mapping in Panama. Photogramm. Engg, 35(7), 641-6.

DALKE, G.W., 1969 - Regional slopes with non-stereo radar. Photogramm. Engg, 35(5), 446-52.

DE AZEVEDO, L.H.A., 1971 - Radar in the Amazon. Proc. 7th Symp. Remote Sensing of Environment. Univ. Michigan, Ann Arbor, 2303-6.

DELLWIG, L.F., 1969 - An evaluation of multifrequency radar imagery of the Pisgah Crater area, California. Mod. Geol., 1(1), 65-73.

DELLWIG, L.F., KIRK, J.N., & WALTERS, R.L., 1966 - The potential of low-resolution radar imagery in regional geologic studies. J. Geophys. Res., 71(20), 4995-8.

DELLWIG, L.F., MACDONALD, H.C., & KIRK, J.N., 1968 - The potential of radar in geological exploration. Proc. 5th Symp. Remote Sensing of Environment, Univ. Michigan, Ann Arbor, 747-63.

DELLWIG, L.F., MACDONALD, H.C., & KIRK, J.N., 1970 - Three dimensional radar imagery. Photogramm. Engg, 36(9), 987-8.

DELLWIG, L.F., & MOORE, R.K., 1966 - The geological value of simultaneously produced like- and cross-polarized radar imagery. J. Geophys. Res. 71(14), 3597-601.

DE LOOR, G.P., 1969 - Possibilities and uses of radar and thermal infra-red systems. Photogrammetria, 24(2), 43-58.

ELLERMEIER, R.D., FUNG, A.K., & SIMONETT, D.S., 1966 - Some empirical and theoretical interpretations of multiple-polarization radar data. Proc. 4th Symp. Remote Sensing of Environment, Univ. Michigan, Ann Arbor, 657-71.

ELLERMEIER, R.D., SIMONETT, D.S., & DELLWIG, L.F., 1967 - The use of multiparameter radar imagery for the discrimination of terrain characteristics. 1967 IEEE Int. Conv. Rec., 15(2), 127-35.

EPPES, T.A., & ROUSE, J.W. jr., 1974 - Viewing-angle effects in radar images. Photogramm. Engg, 40(2), 169-73.

FEDER, A.M., 1960 - Interpreting natural terrain from radar displays. Photogramm. Engg, 26(4), 618-30.

FIORE, C., 1967 - Side-looking radar restitution. Photogramm. Engg, 33(2), 215-21.

GOODYEAR AEROSPACE CORPORATION, 1969 - Basic concepts of synthetic-aperture, side-looking radar. GIB 9167.

GRAHAM, L.C., 1970 - Earth resources radar for a remote sensing system. Technical proposal. Goodyear Aerospace Co. GAP-4947, 62 pp (unpubl.).

HACKMAN, R.J., 1967 - Geologic evaluation of radar imagery in southern Utah. U.S. Geol. Surv. prof. Pap. 575 D, 135-42.

HARGER, R.O., 1970 - Synthetic aperture radar systems: theory and design. N.Y., Academic Press.

HARTMAN, R.R., & BRENNAN, P.A., undated - Synthetic aperture SLAR: geologic mapping in South America. Litton Aero Service, (unpubl.).

HOFFMAN, P., 1960 - Progress and problems in radar photo interpretation. Photogramm. Engg, 31(4), 612-30.

HOLMES, R.F., 1967 - Engineering materials and side-looking radar. Photogramm. Engg, 33(7), 767-770.

INNES, R.B., 1968 - An interpreter's perspective on modern airborne radar imagery. Proc. 5th Symp. Remote Sensing of Environment, Univ. Michigan, Ann Arbor, 107-22.

KATZ, I., 1966 - Wavelength dependence of the radar reflectivity of the earth and the moon. J. Geophys. Res., 71, 361-6.

LA PRADE, G., 1963 - An analytical and experimental study of stereo for radar. Photogramm. Engg, 29(2), 294-300.

LEBERL, F., 1970 - Metric properties of imagery produced by SLAR and IRLS. Proc. ISP Commiss. IV Symp. Publ. ITC, Delft.

LEVINE, D., 1960 - Radargrammetry. N.Y., McGraw-Hill.

LEWIS, A.J., & MACDONALD, H.C., 1970a - Interpretative and mosaicking problems of SLAR imagery. Remote Sensing of Environment, 1(4), 231-6.

LEWIS, A.J., & MACDONALD, H.C., 1970b - Significance of estuarine meanders identified from radar imagery of eastern Panama and northwestern Columbia. Mod. Geol., 1(3), 187-96.

LEWIS, A.J., & WAITE, W.P., 1973 - Radar shadow frequency. Photogramm. Engg, 34(2), 189-96.

LYON, R.J.P., MERCADO, J., & CAMPBELL, R., 1970 - Pseudo radar. Photogramm. Engg, 36(12), 1257-61.

MACDONALD, H.C., 1969 - Geological evaluation of radar imagery from Darien Province, Panama. Mod. Geol., 1(1), 1-63.

MACDONALD, H.C., KIRK, J.N., DELLWIG, L.F., and LEWIS, A.J., 1969 - The influence of radar look-direction on the detection of selected geological features. Proc. 6th Symp. Remote Sensing of Environment, Univ. Michigan, Ann Arbor, 637-50.

MACDONALD, H.C., & LEWIS, A.J., 1969 - Applications of radar imagery in geologic and geomorphic reconnaissance of tropical environments. J.Geol. Soc. Amer. Abs. Pt 2, 18-19.

MACDONALD, H.C., LEWIS, A.J., & WING, R.S., 1971 - Mapping and landform analysis of coastal regions with radar. Geol. Soc. Amer. Bull. 82(2), 345-58.

MACDONALD, H.C., & WAITE, W.P., 1971 - Optimum depression angles for geological analysis. Mod. Geol., 2(3), 179-93.

MEKEL, J.F.M., 1972 - The geological interpretation of radar images. ITC Textbook of Photointerpretation, Vol. 8, Chapter 2. Enschede, The Netherlands, International Institute for Aerial Survey and Earth Science.

MEYER, M.A., 1966 - Remote sensing of ice and snow thickness. Proc. 4th Symp. Remote Sensing of Environment, Univ. Michigan, Ann Arbor, 183-92.

MOORE, R.K., 1969 - Heights from simultaneous radar and infrared. Photogramm. Engg., 35(7), 649-651.

MOORE, R.K., ROUSE, J.W. jr., 1967 - Electronic processing of synthetic aperture array radar - Proc. IEEE, 55, 233-4.

MOORE, R.K., & THOMANN, G.C., 1971 - Imaging radars for geoscience use. IEEE Trans. Geosci. Electron., GE-9, 155-64.

MOORE, R.K., WAITE, W.P., & ROUSE, J.W., 1969 - Panchromatic and polypanchromatic radar. Proc. IEEE, 57, 590-3.

MORAIN, S.A., & SIMONETT, D.S., 1967 - K-band radar in vegetation mapping. Photogramm. Engg, 32(7), 730-40.

NEWBRY, L.E., 1960 - Terrain radar reflectance study. Photogramm. Engg, 26(4), 630-7.

NORVELLE, F.R., 1972 - AS-11A Radar Program. Photogramm. Engg, 38(1), 77-82.

ORR, D.G., & QUICK, J.R., 1971 - Construction materials in Delta areas. Photogramm. Engg, 37(4), 337-51.

PIKE, R.W., BRENNAN, P.A., & VESSEL, A.J., 1972 - Photogeology interpretations from conventional photography and X-band SLAR imagery. Aero Service Co., (unpubl.).

REEVES, R.G., 1968 - Radar geology. In: Yearbook of science and Technology. N.Y., McGraw Hill. 322-8.

REEVES, R.G., 1969 - Structural geologic interpretation from radar imagery. Geol. Soc. Amer. Bull., 80(11), 2159-64.

ROSENFIELD, G.H., 1968 - Stereo radar techniques. Photogramm. Engg, 34(6), 587-94.

ROUSE, J.W., jr., 1969 - Arctic ice type identification by radar. Proc. IEEE, 57, 605-11.

RYDSTROM, H.O., 1967 - Interpreting local geology from radar imagery. Bull. Geol. Soc. Amer., 78, 429-35.

RYDSTROM, H.O., 1970a - Capabilities of advanced radar systems for monitoring land resources. Goodyear Aerospace Co., GERA-1604 (unpubl.).

RYDSTROM, H.O., 1970b - Geologic exploration with high resolution radar. Goodyear Aerospace Co., GIB-9193 (unpubl.).

RYDSTROM, H.O., 1970c - Imaging natural features with high resolution radar - Goodyear Aerospace Co., GIB-9195 (unpubl.).

SCHEPS, B.B., 1960 - To measure is to know - Geometric fidelity and interpretation in radar mapping. Photogramm. Engg, 26(4), 637-44.

SIMONETT,D.S., 1968 - Potential of radar remote sensors as tools in reconnaissance geomorphic, vegetation and soil mapping. 9th Int. Cong. Soil Sci. Trans., 4(29), 21-80.

SIMONETT, D.S., 1970 - Remote sensing with imaging radar. Geoforum, 2, 61-74.

SIMONS, J.H., 1965 - Some applications of side-looking airborne radar. Proc. 3rd Symp. Remote Sensing of Environment, Univ. Michigan, Ann Arbor, 563-73.

SIMONS, J.H., 1966 - Some applications of side-looking airborne radar. In Selected papers on remote sensing. Amer. Soc. Photogramm., 205-13.

SKOLNIK, M.I. (ed.), 1970 - Radar handbook. N.Y., McGraw-Hill.

SWAIN, G., 1974 - Side-looking radar in geological exploration. Electronics Aust., 35(10), 44-5.

TAYLOR, R.C., 1959 - Terrain return measurements at X, Ku and Ka bands. IRE Nat. Conv. Rec., 1(7), 19-26.

TOMIYASU, K., 1974 - Remote sensing of the earth by microwaves. Proc. IEEE, 62(1), 86-92.

U.S. DEPARTMENT OF DEFENSE, 1967 - Image interpretation handbook, Vol. I. U.S. Government Printing Office, TM 30-245, NAVAIR 10-35-685, AFM 200-50.

VESSEL, A.J., 1971 - Soils interpretation from conventional photography and X-band SLAR imagery - Aero Service Co., (unpubl.).

VIKSNE, A., LISTON, T.C., & SAPP, C.D., 1969 - SLR reconnaissance of Panama. Geophysics, 34(1), 54-64.

WAITE, W.P., & MACDONALD, H.C., 1970 - Snowfield mapping with K-band radar. J. Remote Sensing, 2(2), 143-50.

WASIELEWSKI, J.E., CULOCCIO, T.L., & DI CAPRIO, G.R., 1973 - Holography, radar data and interpreter performance. Photogramm. Engg, 39(6), 617-20.

WING, R.S., 1970 - Cholame area, San Andrea Fault zone, California - A study in SLAR. Mod. Geol., 1(3), 173-86.

WING, R.S., 1971 - Structural analysis from radar imagery: Eastern Panamanian Isthmus. Mod. Geol., 2(1), 1-21 and 75-127.

WING, R.S., & DELLWIG, L.F., 1970 - Radar expression of Virginia Dale Precambrian ring-dike complex, Colorado-Wyoming. Geol. Soc. Amer. Bull., 81(1), 293-8.

WING, R.S., and MACDONALD, H.C., 1973 - Radar geology - Petroleum exploration technique, eastern Panama and northwestern Columbia. Amer. Ass. Petrol. Geol. Bull., 57(5), 825-40.

WING, R.S., OVERBEY, W.K., & DELLWIG, L.F., 1970 - Radar lineament analysis, Burning Springs area, West Virginia - An aid in the definition of Appalachian Plateau Thrusts. Geol. Soc. Amer. Bull., 81(11) 3437-44.

WISE, D.U., 1967 - Radar geology and pseudo-geology. Geology of an Appalachian Piedmont cross-section. Photogramm. Engg, 33(7), 753-61.

# PLATE 1 — MOUNT ISA TEST AREA

## A — PRELMINARY SLAR INTERPRETATION


REFERENCE

- Main drainage
- Boundary
- Fault
- Lineament
- Joint sets
- Dips
- Dyke
- Trend line

PLATE 1, A :

| SLAR units | Possible geological equivalents | Equivalent rock types |
|---|---|---|
| 1. Flat. Scarce to moderately abundant, dendritic drainage. Some long lineaments. Dark to very dark tone. Mottled texture. | Poorly resistant or weathered rocks, alluvium | 1, 2; some 4, 6 |
| 2. Mesa-like relief, dissected in places. Fractured in places. Scarce, dendritic drainage. Medium tone. Mottled texture. | Recent, poorly consolidated sandstone and/or siltstone | 4 in western part of area |
| 3. High relief. Distinctly bedded, formed by alternating hard and soft layers. Abundant, mainly consequent drainage. Moderately fractured. Very high reflectivity probably due to abundance of corner reflectors. Coarse texture. | Quartzite, sandstone with interbedded shale, schist | 3; some 4, 5 |
| 4. Similar to 3, but less distinctly bedded | Quartzite, sandstone | 3, 4; some 5, 6 |
| 5. Low to very low relief. Bedding or lineation clearly shown by tone variations. Some fractures. Moderately abundant drainage, generally dendritic but in some places structurally controlled. Average tone is dark. Texture is generally streaked, but mottled in places | Soft sedimentary or low-grade metamorphic rocks | 5; some 3, 4 |
| 6. Low to very low relief, massive. Very fractured. Very scarce, dendritic drainage. Medium grey tone. Mottled texture. | Intrusive rocks | 6 |
| 7. High relief. Smooth, rounded hills separated by deep narrow valleys. Very few fractures. Dense drainage. Light tone. Smooth, uniform texture. | Massive quartzite | 3; some 5 |
| 8. Small outcrops lacking distinctive characters. | ? ? ? | Various |

## B — LITHOLOGICAL MAP

MOUNT ISA 1:100 000 MAP | MARY KATHLEEN 1:100 000 MAP

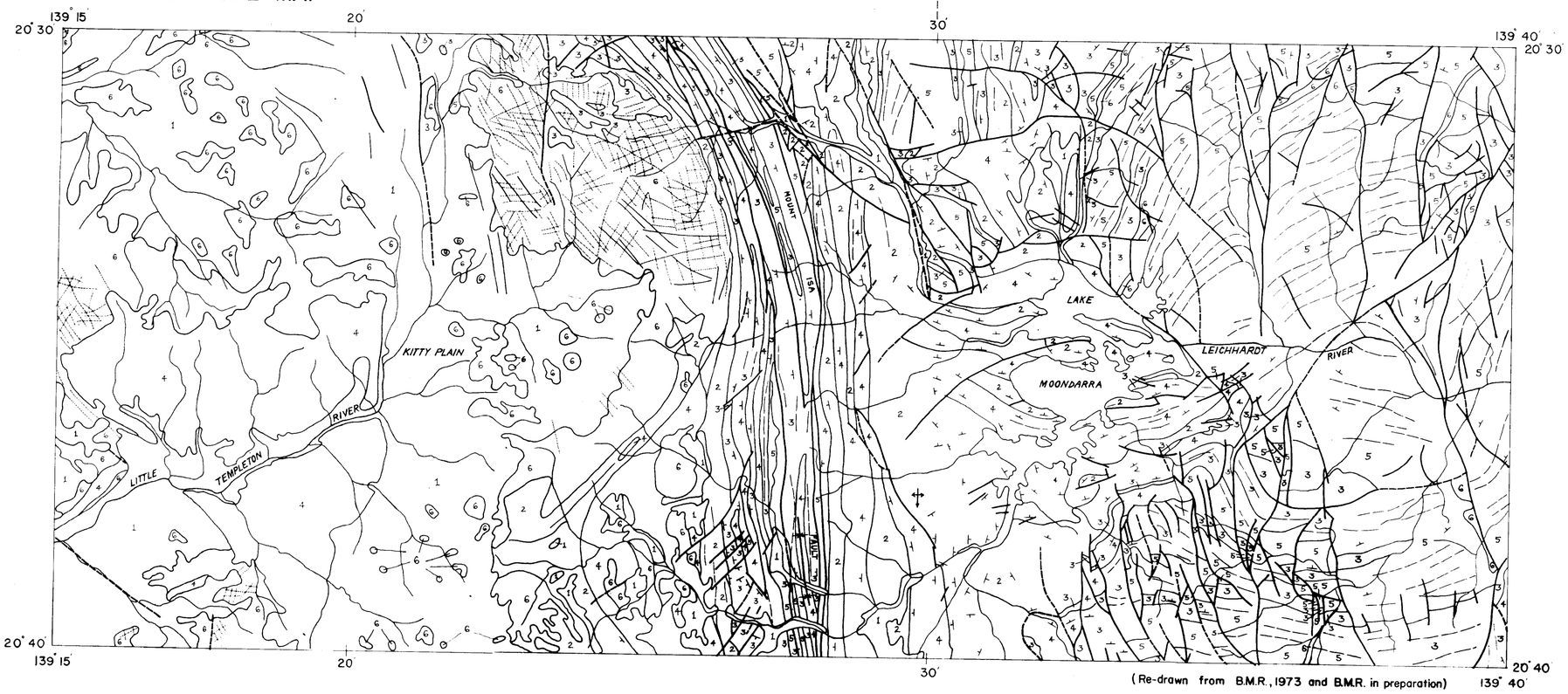


(Re-drawn from B.M.R., 1973 and B.M.R. in preparation)

PLATE 1, B:

| Rock types | Letter symbols of equivalent rock units Mt Isa Sheet (BMR 1973) | Mary K. Sheet (BMR in prep.) |
|---|---|---|
| 1. Soil, sand, alluvium | Cza, Czb, Czg, Czr | Cz |
| 2. Dolomite, dolomitic siltstone, dolomitic quartzite | Pik, Pis, Pin, Pim | Pik, Pis, Pin, Pim |
| 3. Quartzite, sandstone, conglomerate; minor siltstone, schist, shale | $Phj_1$, Phg, $Phm_1$ | $Pr_q$, $Piw_3$, $Phm_3$, $Phm_2$, $Phm_1$, $Phl_3$, $Phg_2$, $Phg_1$ |
| 4. Shale, siltstone, schist; minor chert, conglomerate | Cmi, Cme, $Phj_2$, $Phe_s$, Pig, Piu, Pib | Piu, Pib, $Pr_t$, $Piw_2$ |
| 5. Metabasalt; minor tuff, quartzite, sandstone | $Phj_3$, Phe, $Phe_b$, $Phe_a$, Php, $Phc^b$ | Php, Phc, $Phc_q$ |
| 6. Granite, dolerite | $Pgs_3$, $Pgs_2$, $Pgs_1$; do | do |

PLATE 1, C:

WEST OF MT ISA FAULT

Rock units from BMR 1973

CAINOZOIC

- Cz — Soil, sand, and alluvium

PALAEOZOIC - CAMBRIAN

- Inca Formation / Beetle Creek Formation — Cmi — Siliceous shale and chert with limestone interbeds; Cme — Basal conglomerate, chert, siliceous shale with trilobite fossils
- Sybella Granite — $Pgs_3$ — Massive fine to medium even-grained granite; $Pgs_2$ — Coarse porphyritic foliated biotite granite; $Pgs_1$ — Massive medium to coarse porphyritic granite
- do — Dolerite, metadolerite, amphibolite

PROTEROZOIC - CARPENTARIAN

- $Phj_2$ — Siltstone, shale, pelitic schist, quartz-muscovite schist
- Judenan Beds — $Phj_1$ — White quartzite, feldspathic quartzite, foliated quartzite, minor schist
- Eastern Creek Volcanics — Phe — Undivided : metabasalt, amygdaloidal metabasalt, amphibolite; $Phe_b$ — Metabasalt, amygdaloidal metabasalt, amphibolite; $Phe_s$ — Pelitic schist, cordierite-schist, quartzite; $Phe_a$ — Metabasalt, amygdaloidal metabasalt, amphibolite

## C — FIELD INFORMATION AND FINAL SLAR INTERPRETATION

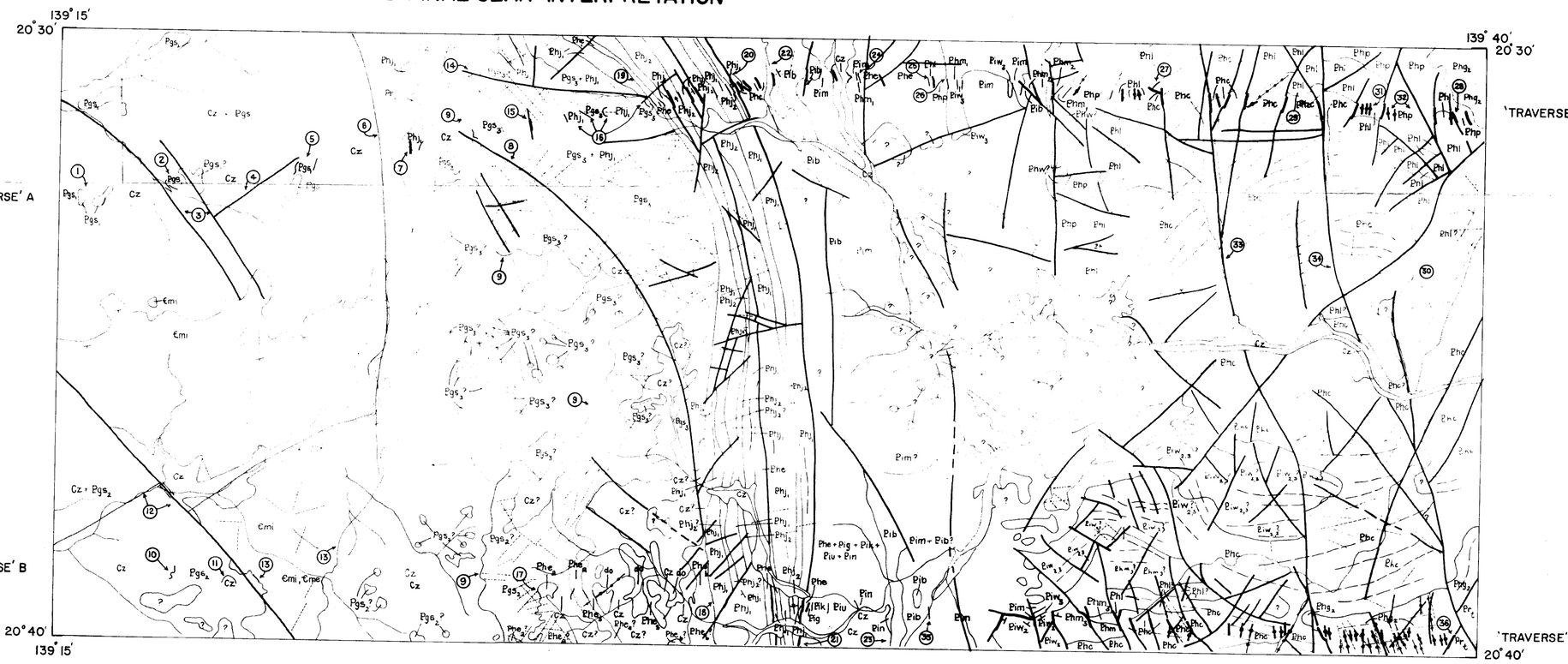


SCALE 1:100,000

EAST OF MT ISA FAULT

Rock units from BMR 1973 and BMR in prep.

CAINOZOIC

- Cz — Soil, sand, alluvium

PROTEROZOIC-CARPENTARIAN

- Mt Isa Group, Mary Kathleen Group — Pig — Magazine Shale: Thin bedded calcareous sericitic shales, minor pyrite; Pik — Kennedy Siltstone: Siliceous and dolomitic siltstone, dolomitic quartzite; Piu — Urquhart Shale: Ferruginous pyritic shale, tuff marker beds; Pin — Native Bee Siltstone: Bedded dolomitic siltstone, minor tuff; Pib — Breakaway Shale: Grey shale, minor siltstone; $Pr_t$ — Siltstone and shale; Pim — Moondarra Siltstone: Dolomitic siltstone, minor dolomite and shale; $Piw_3$ — Warrina Park Quartzite: Orthoquartzite, conglomerate; $Piw_2$ — Warrina Park Quartzite: Orthoquartzite, siltstone
- Phm — Myally Beds, Undivided: quartzite, siltstone, shale, conglomerate; $Phm_3$ — Myally Beds: Feldspathic quartzite, conglomerate; $Phm_2$ — Myally Beds: Fine feldspathic quartzite, grey siltstone; $Phm_1$ — Myally Beds: Feldspathic sandstone, quartzite, mud-flake conglomerate
- Haslingden Group — Phe — Eastern Creek Volcanics, Undivided: Metabasalt, amygdaloidal metabasalt, amphybolite; Php — Eastern Creek Volcanics, Pickwick Metabasalt Member: Metabasalt, amygdaloidal metabasalt; Phl — Eastern Creek Volcanics, Lena Quartzite Member: Quartzite, feldspathic quartzite; Phc — Eastern Creek Volcanics, Cromwell Metabasalt Member: Metabasalt, amygdaloidal metabasalt, flowtop breccia; $Phg_2$ — Mt Guide Quartzite: Quartzite, feldspathic sandstone, limonitic sandstone; $Phg_1$ — Mt Guide Quartzite: Fine to medium sandstone, siltstone, arkose

Full tone : information from BMR 1973 and BMR in prep. ('traverses' A and B)

Half tone : SLAR interpretation

(35) : point of interest, discussed in text

Record: 74/150

F 54(A)32